Article

TRANSPARENT PROCESS

THE EMBO JOURNAL

Evi1 regulates Notch activation to induce zebrafish hematopoietic stem cell emergence

Martina Konantz[1,†], Elisa Alghisi[1,†], Joëlle S Müller[1], Anna Lenard[1], Virginie Esain[2], Kelli J Carroll[2], Lothar Kanz[3], Trista E North[2,4] & Claudia Lengerke[1,3,5,*]

Abstract

During development, hematopoietic stem cells (HSCs) emerge from aortic endothelial cells (ECs) through an intermediate stage called hemogenic endothelium by a process known as endothelial-to-hematopoietic transition (EHT). While *Notch* signaling, including its upstream regulator *Vegf*, is known to regulate this process, the precise molecular control and temporal specificity of Notch activity remain unclear. Here, we identify the zebrafish transcriptional regulator *evi1* as critically required for Notch-mediated EHT. *In vivo* live imaging studies indicate that *evi1* suppression impairs EC progression to hematopoietic fate and therefore HSC emergence. *evi1* is expressed in ECs and induces these effects cell autonomously by activating Notch via pAKT. Global or endothelial-specific induction of *notch*, *vegf*, or pAKT can restore endothelial Notch and HSC formations in *evi1* morphants. Significantly, *evi1* overexpression induces Notch independently of Vegf and rescues HSC numbers in embryos treated with a Vegf inhibitor. In sum, our results unravel *evi1*–pAKT as a novel molecular pathway that, in conjunction with the *shh*–*vegf* axis, is essential for activation of Notch signaling in VDA endothelial cells and their subsequent conversion to HSCs.

Keywords AKT; endothelial-to-hematopoietic transition; EVI1; hematopoietic stem cells; Notch; VEGF

Subject Categories Development & Differentiation; Signal Transduction; Stem Cells

DOI 10.15252/embj.201593454 | Received 9 November 2015 | Revised 11 August 2016 | Accepted 23 August 2016 | Published online 16 September 2016

The EMBO Journal (2016) 35: 2315–2331

Introduction

The zebrafish (*Danio rerio*) model is increasingly used to study vertebrate hematopoiesis. Its rapid development, external fertilization, and embryonic transparency facilitate *in vivo* imaging of early embryonic processes and make it amenable for genetic and small molecule screens (Palis & Yoder, 2001; Davidson & Zon, 2004; Bertrand & Traver, 2009). Moreover, molecular pathways governing blood development appear largely conserved between fish and mammals, indicating that knowledge obtained in this model is likely transferrable to mammalian systems. As in other vertebrates, zebrafish hematopoiesis develops in sequential waves (Davidson & Zon, 2004). The first hematopoietic cells appear as the primitive wave at 12 h post-fertilization (hpf) in the intermediate cell mass, an intra-embryonic tissue derived from the ventral mesoderm (Detrich *et al*, 1995; Palis & Yoder, 2001). A second transient hematopoietic wave occurs in the caudal hematopoietic tissue (CHT), where multipotent erythromyeloid progenitors (EMPs) are generated as early as 24 hpf (Bertrand *et al*, 2007, 2010b). Shortly afterward, these cells are replaced by definitive hematopoietic stem/progenitor cells (HSPCs) that in fish start emerging approximately at 26 hpf in the ventral dorsal aorta (VDA)—the equivalent of the aorta–gonad–mesonephros (AGM) region in mammals—and then migrate to the CHT to expand in number (Bertrand *et al*, 2010a; Boisset *et al*, 2010). HSPCs subsequently colonize kidney marrow and thymus, the adult hematopoietic organs, to maintain the hematopoietic pool throughout the zebrafish life span (Jin *et al*, 2007; Chen & Zon, 2009).

The regulation of HSPC development in the VDA and AGM, respectively, is subject of intense research. On the cellular level, HSPCs arise from specialized VDA endothelial cells (ECs) referred to as hemogenic endothelium (HE), in a process known as endothelial-to-hematopoietic transition (EHT). Molecularly, several signaling pathways and genes have been demonstrated to regulate both artery and HSPC development (North *et al*, 1999; Burns *et al*, 2009; Chen *et al*, 2009). For example, the Notch–gridlock pathway controls the assembly of the first embryonic arteries, regulates arterial endothelial fate specification, and is critical for definitive hematopoietic stem cell (HSC) formation in both mammals and fish (Zhong *et al*, 2001; Kumano *et al*, 2003; Burns *et al*, 2005; Robert-Moreno *et al*, 2005). Interestingly, Notch signaling is dispensable for the specification of primitive hematopoietic cells and EMPs (Bertrand *et al*, 2010b). Although arterial identity has been described as a

1 Department of Biomedicine, University Hospital Basel, Basel, Switzerland
2 Beth Israel Deaconess Medical Center, Harvard Medical School, Boston, MA, USA
3 Department of Internal Medicine II, University Hospital Tuebingen, Tuebingen, Germany
4 Harvard Stem Cell Institute, Cambridge, MA, USA
5 Division of Hematology, University Hospital Basel, Basel, Switzerland
*Corresponding author. Tel: +41 61 55 65129; E-mail: claudia.lengerke@unibas.ch
† These authors contributed equally to this work

prerequisite for HSCs, it is still controversial whether full arterial specification is required for HSC generation (de Bruijn *et al*, 2000). Indeed, most of the mouse and fish mutants that do not generate arteries show defective HSC development (Kumano *et al*, 2003; Burns, 2005; Robert-Moreno *et al*, 2008; North *et al*, 2009). However, hematopoiesis is not necessarily affected in mutants with perturbed artery–vein boundaries, if intact Notch signaling is provided (Burns *et al*, 2005; You *et al*, 2005). Together, these data suggest that active Notch signaling is a key factor for ECs to generate HSCs, as well as needed for full arterial specification. Precise Notch activity levels, as achieved in ECs of the VDA at this developmental time point, might in fact distinguish cells capable of differentiating into blood from those that do not have this property and will remain part of the arteries (Gama-Norton *et al*, 2015). Supporting this notion, *in vitro* cultured ECs derived from murine AGM, human embryonic stem (hES), or *Macaca nemestrina*-induced pluripotent stem (iPS) cells require Notch induction (e.g., via genetic manipulation or co-culture with ECs expressing the Notch ligands *Jag1* and *Dll4*) for generating definitive HSPCs (Gori *et al*, 2015; Hadland *et al*, 2015). Similarly, the Notch ligand *Dll4* was implicated as a hemato-endothelial progenitor marker in hESCs and shown to regulate their hematopoietic differentiation (Ayllón *et al*, 2015).

The upstream regulatory mechanisms that control Notch levels in ECs are not fully understood. A major inductive role has been attributed to vascular endothelial growth factor (Vegf) and its upstream regulator sonic hedgehog (Ssh), which both have an essential role in regulating zebrafish HSC development in a Notch-dependent manner (Lawson *et al*, 2002; Gering & Patient, 2005). However, in contrast to direct exposure to Notch ligands (Gori *et al*, 2015), standard addition of Vegf to cultured ES cells cannot by itself induce HSCs (Lengerke & Daley, 2005, 2010; Lengerke *et al*, 2008; Müller & Lengerke, 2009), indicating that additional factors may be involved in Notch regulation. Here, we identify the zebrafish homologue of the zinc finger transcription factor ecotropic viral integration site-1 (Evi1, also termed Mecom) as a critical regulator of Notch pathway induction and HSC emergence in the zebrafish VDA endothelium.

Evi1 is a member of the SET/PR domain protein family and contains ten zinc finger motifs organized into two domains, each with distinct DNA-binding specificities (Fig EV1A; Perkins *et al*, 1991; Delwel *et al*, 1993). Given its complex molecular structure, Evi1 can interact with different molecular partners, exerting inductive and/or repressive effects on several genes in a tissue-dependent manner (Wieser, 2007). Identified several years ago as a common locus of retroviral integration in murine myeloid tumors (Mucenski *et al*, 1988), *Evi1* has been mostly studied as an oncogene and poor risk factor in leukemia (Suzukawa *et al*, 1994; Ogawa *et al*, 1996; Konantz *et al*, 2013). However, *Evi1* is also expressed in several embryonic and adult tissues (e.g., heart, somites, cranial ganglia, peripheral nervous system) and regulates proliferation and/or differentiation of various cell types (Hirai, 1999; Wieser, 2007). *Evi1*$^{-/-}$ mice die early, between 10.5 (Hoyt *et al*, 1997; Yuasa *et al*, 2005) and 16.5 (Goyama *et al*, 2008) days post-coitum, depending on the model, and show multiple abnormalities including paleness and reduced numbers of proliferating HSCs (Hoyt *et al*, 1997; Yuasa *et al*, 2005; Goyama *et al*, 2008). Here, we use the zebrafish model to investigate the mechanistic role of *evi1* in developmental hematopoiesis. We find that *evi1* regulates EHT and is required for the generation of HSPCs in the VDA. Molecularly, *evi1* regulates this process by inducing pAKT-Notch independently of Vegf activation.

Results

Zebrafish *evi1* expression is detectable in the VDA and required for HSC development

Whole-mount *in situ* hybridization (WISH) analyses were performed to document expression of the zebrafish homologue of the *evi1* gene during early zebrafish development. Consistent with data collected in mice (Hoyt *et al*, 1997), *evi1* expression is detectable in select cell types in the brain, the branchial arches, and the posterior pronephric duct (Fig 1A left and middle). Moreover, *evi1* is expressed in the zebrafish VDA at the time point of HSC emergence and co-localizes with the endothelial marker *flk1* (Fig 1A right) and the HSC marker *c-myb* (Appendix Fig S1), as shown by double WISH (Davidson & Zon, 2004). These results suggest that *evi1* is present in hematopoietic cells as they emerge from the aortic endothelium and may regulate definitive hematopoiesis in a cell-autonomous manner.

Figure 1. *evi1* is expressed in emerging HSPCs and critically regulates definitive hematopoiesis.

A Whole-mount *in situ* hybridization (WISH) of *evi1* at 20 (left) and 32 (middle) hpf. *evi1* expression is visible in various structures of the brain, neuronal structures, the posterior pronephric duct (ppnd), and the branchial arches (ba), as well as in the VDA (ventral dorsal aorta) region. Additionally, *evi1* co-localizes with the endothelial marker *flk1* (right).

B, C WISH of *runx1/c-myb* in HSPCs (B), *mpo* in neutrophils (left), and *l-plastin* (right) in monocytes/macrophages (C) at 36 hpf in control (upper)- and *evi1* MO (lower)-injected embryos.

D–G WISH of *globin* in erythrocytes of 6 dpf embryos (D), of *rag-1* in the thymus of 5 dpf embryos (E; red asterisk), of *cd41* at 52 hpf (F), and *gata2b* at 32 hpf (G) for both control (upper)- and *evi1* morpholino (lower)-injected embryos.

H Quantitation of results is shown for each gene, displaying the percentages of embryos with normal vs. changed expression in each condition. A Fisher's exact test was applied to calculate statistical significance. ***$P < 0.001$.

I WISH of *runx1/c-myb* in HSPCs of uninjected control and *UAS:mEvi1* plasmid DNA-injected *Tg(-1.5hsp70l:Gal4)* embryos with heat-shock induction performed at 14 hpf.

J WISH of *runx1/c-myb* in HSPCs of uninjected control and *UAS:mEvi1* mRNA in *Tg(fli.1:Gal4FF;UAS:RFP)* embryos, leading to endothelial-specific *evi1* overexpression.

K Graph displays quantitation of results from (I) and (J), displaying the percentages of embryos with normal vs. changed expression in each condition. A Fisher's exact test was applied to calculate statistical significance. **$P < 0.01$, ***$P < 0.001$.

Data information: Lateral views are shown, with anterior to the left, dorsal up. Numbers indicate the amount of embryos with the respective phenotype/total number of embryos analyzed in each experiment. Arrows indicate up- or downregulation for each gene. A minimum of two biological replicates was performed for each marker with at least $n = 5$ embryos per experiment.

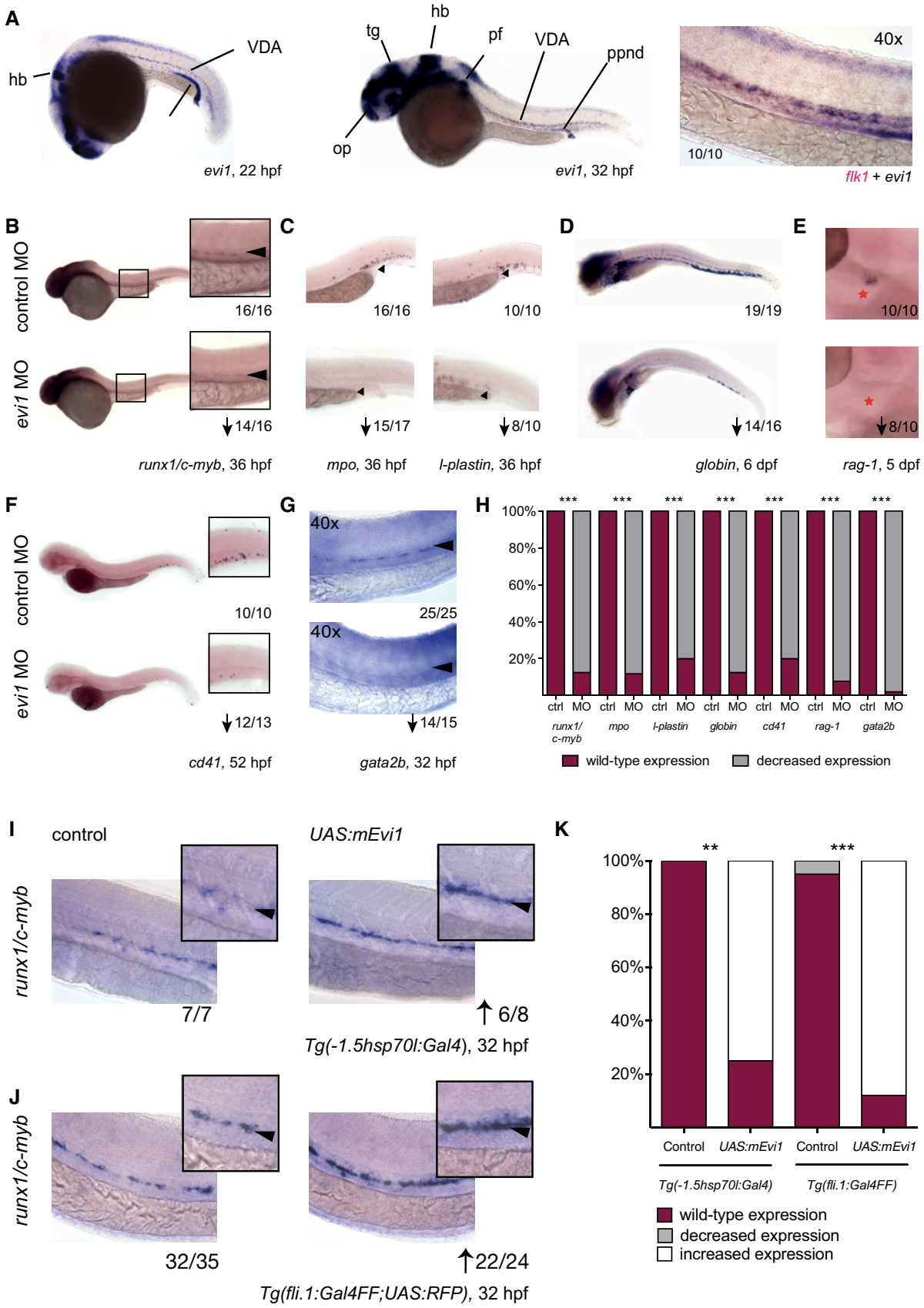
A
hb
VDA
evi1, 22 hpf
tg
hb
pf
VDA
ppnd
op
evi1, 32 hpf
40x
10/10
flk1 + evi1
B
control MO
evi1 MO
16/16
14/16
runx1/c-myb, 36 hpf
C
16/16
10/10
15/17
8/10
mpo, 36 hpf
l-plastin, 36 hpf
D
19/19
14/16
globin, 6 dpf
E
10/10
8/10
rag-1, 5 dpf
F
control MO
evi1 MO
10/10
12/13
cd41, 52 hpf
G
40x
25/25
40x
14/15
gata2b, 32 hpf
H
100%
80%
60%
40%
20%
ctrl MO ctrl MO ctrl MO ctrl MO ctrl MO ctrl MO ctrl MO
runx1/ c-myb
mpo
l-plastin
globin
cd41
rag-1
gata2b
wild-type expression
decreased expression
I
control
UAS:mEvi1
runx1/c-myb
7/7
6/8
Tg(-1.5hsp70l:Gal4), 32 hpf
J
runx1/c-myb
32/35
22/24
Tg(fli.1:Gal4FF;UAS:RFP), 32 hpf
K
**
***
100%
80%
60%
40%
20%
Control
UAS:mEvi1
Control
UAS:mEvi1
Tg(-1.5hsp70l:Gal4)
Tg(fli.1:Gal4FF)
wild-type expression
decreased expression
increased expression

Figure 1.

To investigate the role of *evi1* in zebrafish hematopoiesis, *in vivo* loss-of-function experiments were performed and embryos treated with two different antisense morpholino oligonucleotides (MO) to inhibit *evi1* pre-mRNA splicing. Both MOs result in intron preservation, thereby leading to a premature stop either in the 2nd (MO1) or the 6th (MO2) zinc finger of the first zinc finger domain (Fig EV1A and B). Transcripts in morphants were mis-spliced, whereas uninjected and control-injected embryos showed normal splicing (Fig EV1C). *o*-Dianisidine staining was performed to exclude major defects in vascular integrity, including hemorrhaging and/or blood pooling, in MO-injected fish (Fig EV1D). Control and *evi1* MO-injected fish were analyzed by WISH for the expression of hematopoietic genes and/or flow cytometric quantification using transgenic reporter lines (Fig 1B–H and Appendix Fig S2). Indeed, reduced numbers of *runx1*$^+$/*c-myb*$^+$ HSPCs were observed in the VDA region of *evi1* morphants vs. control embryos at 36 hpf (Figs 1B and H, and EV2A and C). Co-injection with zebrafish *evi1* mRNA in wild-type fish (Fig EV1E) and, respectively, with *UAS:mEvi1* plasmid DNA in *Tg(fli.1:Gal4FF;UAS:RFP)* fish (Fig EV1E'), was able to rescue *runx1/c-myb* expression in the VDA of *evi1* morphants, indicating that the observed effects on HSCs were specific to *evi1* inhibition.

Consistent with HSPC loss, lower numbers of *mpo*$^+$, *l-plastin*$^+$, or *lyz*$^+$ myeloid cells (Fig 1C and Appendix Fig S2A, *Tg(lyz:dsred)*: $P = 0.0286$) as well as *hbae3*$^+$, *globin*$^+$ erythroid cells (Fig 1D and Appendix Fig S2B, *Tg(globin:GFP)*: $P = 0.057$), *rag1*$^+$ T lymphocytes (Fig 1E, note that thymus epithelium is intact as shown in Fig EV3A), and *cd41*$^+$ cells (Fig 1F and Appendix Fig S2C, *Tg(cd41:eGFP)*: $P = 0.0286$) were documented by WISH and flow cytometry in *evi* morphants vs. control fish analyzed at 36 hpf to 6 dpf (Figs 1C–H and EV2B and C). Interestingly, we also observe downregulation of *gata2b,* a recently identified early regulator of the HE (Butko *et al*, 2015), in our *evi1* morphants (Fig 1G). Together, these data suggest that suppression of *evi1* expression severely affects VDA-derived HSPCs, thereby strongly reducing blood cell counts of all definitive lineages (Figs 1H and EV2C). Further supporting the notion that *evi1* expression regulates definitive hematopoiesis, increased numbers of HSPCs were observed at 32 hpf in the VDA of *UAS:mEvi1*-injected *Tg(-1.5hsp70l:Gal4)* or *Tg(fli.1:Gal4FF;UAS:RFP)* embryos, in which *Evi1* expression was conditionally induced by heat shock or via the Gal4:UAS binary system specifically in endothelial cells, respectively (Fig 1I–K).

evi1 regulates HSC development by inducing EHT

Next, we explored the mechanism by which *evi1* expression regulates HSPCs. Genes marking the blood vessels (*flt1* and *flt4*, Fig EV3B) and nearby tissues (e.g., *shh* in the notochord, see Fig EV3C) showed unaltered expression. Importantly, circulation was intact in *evi1* morphants, suggesting that the HSPC defect was not due to gross alteration of vascular development or blood flow, previously shown to affect HSC formation (Adamo *et al*, 2009; North *et al*, 2009; Movies EV1, EV2, and EV3). However, *evi1* morphants showed strong reduction in the expression of *notch1b* and *dll4* (Fig 2A), while conditional induction of *Evi1* leads to increased *notch1b* expression (Fig 2B), suggesting that *evi1* might regulate HSCs by modulating Notch activity. Since *evi1* co-stained with the endothelial marker *flk1* in the VDA (Fig 1B), but *evi1* suppression did not overtly impair endothelial cells (Fig EV3B), we asked whether EHT, the next step in HSC development, was perturbed. Double-transgenic *Tg(kdrl:mKate-CAAX;c-myb:eGFP)* embryos were examined by *in vivo* confocal time-lapse microscopy between 28 and 42 hpf, to analyze the emergence of HSPCs (*c-myb:eGFP*$^+$ (green)) from the VDA (*kdrl:mKate*$^+$ (red)). Consistent with the results above, microscopy did not reveal any obvious endothelial phenotype in *evi1* morphants. In control-injected embryos, *c-myb:eGFP*$^+$ hematopoietic cells directly arose from *kdrl:mKate*$^+$ ECs along the VDA as previously described: ECs, normally flattened in appearance, transformed into double-positive *kdrl*$^+$*c-myb*$^+$ cells of spherical shape before budding into the lumen of the DA (Fig 3A, control MO, upper panel) (Bertrand *et al*, 2010a; Kissa & Herbomel, 2010). However, after *evi1* MO injection, *kdrl*$^+$*c-myb*$^+$ cells started transitioning to spherical shape but could not emerge from the DA (Fig 3A, *evi1* MO, lower panel). In particular, endothelial *kdrl*$^+$ cells from the VDA of *evi1* morphants began to turn yellow indicative of acquisition of the green signal due to *c-myb* induction, but afterward failed to be released into the lumen of the venous system as seen in control embryos (see Movie EV1). To quantify these observations, *kdrl*$^+$*c-myb*$^+$ cells detectable at any time in the VDA, their proliferation capacity, as well as numbers of HSPCs directly emerging from *kdrl*$^+$*c-myb*$^+$ cells (as documented by live imaging) were counted in $n = 10$ movies of *evi1* morphants and control embryos, each taken over 8 h. Interestingly, *evi1* MO-injected embryos showed a significantly lower amount of emerging HSPCs than control-injected embryos (Fig 3B, $P < 0.01$), while no differences were detected in dividing or total numbers of *kdrl*$^+$*c-myb*$^+$ cells ("*kdrl*$^+$*c-myb*$^+$ cells in view"). In sum, these data indicate that *evi1* expression is required for full transition to the hematopoietic fate and specifically regulates HSPCs emergence (Fig 3B) from the VDA.

To further investigate the influence of *evi1* during EHT, we isolated *kdrl*$^+$*c-myb*$^+$ cells from *evi1* MO and control *Tg(kdrl:mKate; c-myb:eGFP)* embryos, respectively, by FACS (Appendix Fig S3) and performed qRT–PCR expression analyses of hematopoietic and endothelial genes. *evi1* knockdown quantitatively reduced the *kdrl*$^+$*c-myb*$^+$ cell population (2.59% vs. 1.4% of total gated live embryonic cells, Appendix Fig S3, $P < 0.05$), which comprises the *kdrl*$^+$*c-myb*$^+$ cells in the VDA as well as most of emerging HSPCs, and may retain some fluorescent signal indicative of an endothelial origin (due to the half-life of the introduced fluorescent protein). Interestingly, the *kdrl*$^+$*c-myb*$^+$ cell population of *evi1* morphants also showed severe upregulation of endothelial and downregulation of hematopoietic genes (Fig 3C), indicative of an arrest in the transition from endothelial-to-hematopoietic cell fate. Together, these data argue that *evi1* expression is required for the transition of ECs to hematopoietic fate and thereby for HSC emergence.

HSPC emergence is determined by parallel *evi1* and Vegf-mediated Notch induction

One prominent regulator of early HSC development is the Notch–Runx1 pathway (Burns *et al*, 2005). Although morphologically normal, endothelial cells in the VDA of *evi1* morphants showed strongly reduced expression of *dll4* and *notch1b* (Fig 2A), suggesting that *evi1* might impact HSPC emergence via Notch regulation. Treatment with DAPT, a γ-secretase inhibitor that blocks the

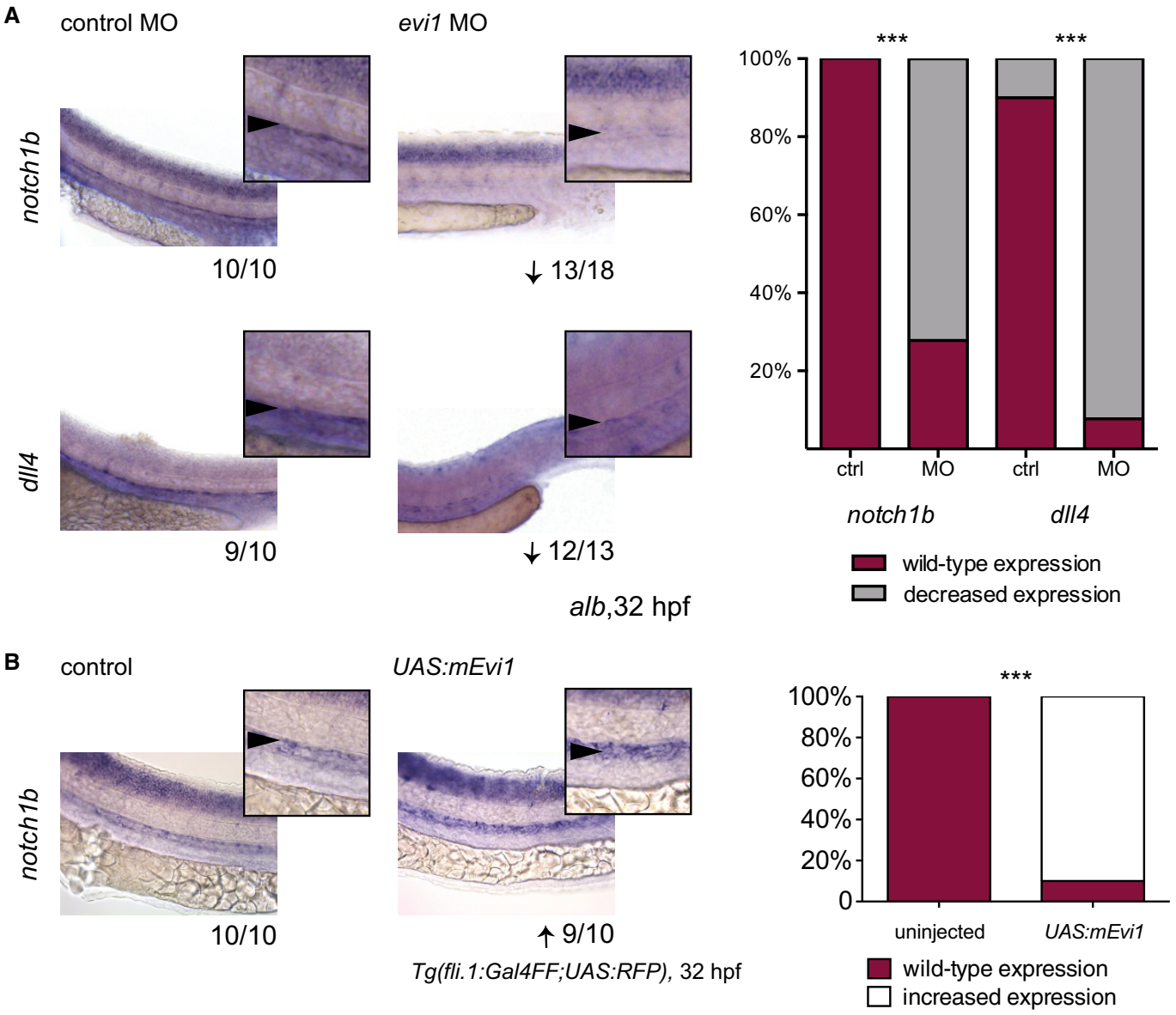

Figure 2. Endothelial Notch signaling is dependent on *evi1* expression levels.

A WISH of *notch1b* (upper) and *dll4* (lower) in both control (left)- and *evi1* MO-injected embryos (right).

B WISH of *notch1b* in uninjected (left) and *UAS:mEvi1* plasmid DNA-injected (right) *Tg(fli.1:Gal4FF;UAS:RFP)* embryos resulting in endothelial-specific *evi1* induction.

Data information: Lateral views are shown, with anterior to the left, dorsal up. Squares represent enlargements of the region of interest. Numbers indicate the amount of embryos with the respective phenotype/total number of embryos analyzed in each experiment. Arrows indicate up- or downregulation for each gene. A minimum of two biological replicates was performed for each marker with at least $n = 5$ embryos per experiment. For each analyzed gene, quantitation of results is shown, displaying the percentages of embryos with normal vs. changed gene expression for each condition. A Fisher's exact test was applied to calculate statistical significance. n.s., not significant; ***$P < 0.001$.

intracellular cleavage of Notch receptors required for signal propagation, strongly inhibited HSPC formation but did not influence *evi1* expression, suggesting that *evi1* is upstream of Notch signaling at this stage of development in the VDA (Appendix Fig S4). However, *evi1* morphants showed unchanged expression of the Notch ligand *delta C* (*dlc*) and the Notch target gene *efnb2a*, a well-established arterial marker commonly associated with HE capable of HSC generation (Fig EV4A and B) suggestive of a more complex regulatory interaction.

To further investigate the relationship between *evi1* and the Notch pathway, we next performed rescue experiments using a heat-shock-inducible *notch intracellular domain* (*NICD*) transgenic zebrafish line. Indeed, defined hyper-activation of *NICD* at both 14 and 20 hpf robustly rescued the loss of *runx1/c-myb* expression in the VDA of *evi1* morphants (Fig 4A and F; Appendix Fig S5A and C). In order to determine whether spatially restricted endothelial expression of NICD was sufficient to rescue HSC development in the VDA of *evi1* suppressed fish, we used an endothelial-specific Gal4 driver

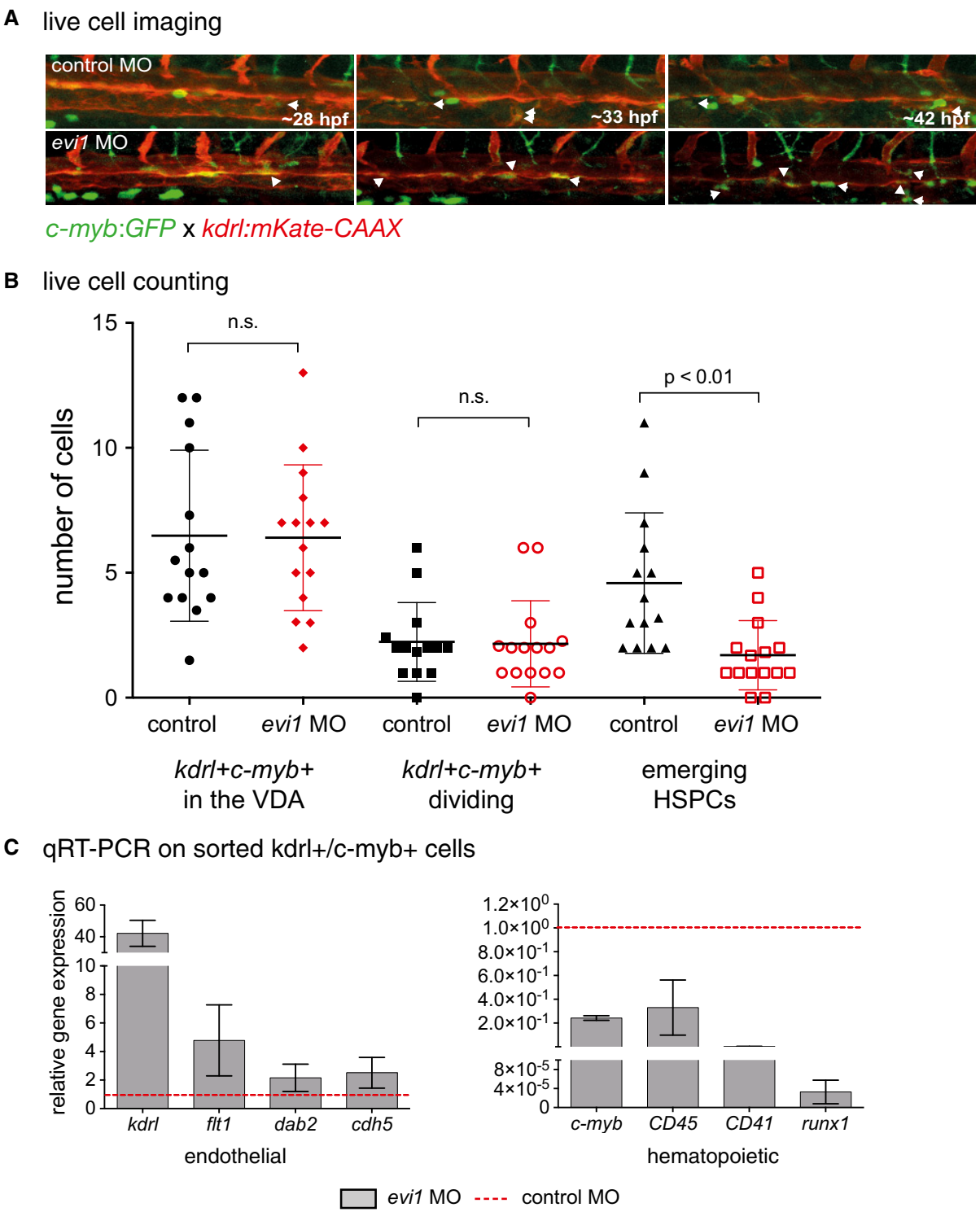

Figure 3. *evi1* regulates HSC emergence from the VDA.

A Confocal time-lapse live imaging was performed in *Tg(c-myb:GFP; kdrl:mKate-CAAX)* embryos from 28 to 42 hpf (Movie EV1). Shown are three representative time points in which the transformation from hemogenic endothelial cells to the hematopoietic fate is visible, indicated by the white arrowheads. For each time point, merged images are shown. White arrowheads denote double-positive cells.

B Cell counts of total numbers of $kdrl^{+}cmyb1^{+}$ cells "in view", dividing and, respectively, emerging HSPCs. n = 10 movies from n = 3 biological replicates were analyzed. A nonparametric Mann–Whitney U-test was used to test for statistical significance, and error bars are shown as ± s.d.

C Gene expression analysis of endothelial (*kdrl, flt1, dab2, cdh5*) and blood-specific genes (*c-myb, CD45, CD41, runx1*) in sorted $kdrl^{+}c\text{-}myb^{+}$ cells from 34 hpf *Tg(c-myb:GFP; kdrl:mKate-CAAX)* embryos. Cells were isolated from 15 to 25 pooled embryos per sample. Three biological experiments were performed with one representative shown. Error bars indicate s.d. of three technical replicates for each representative experiment.

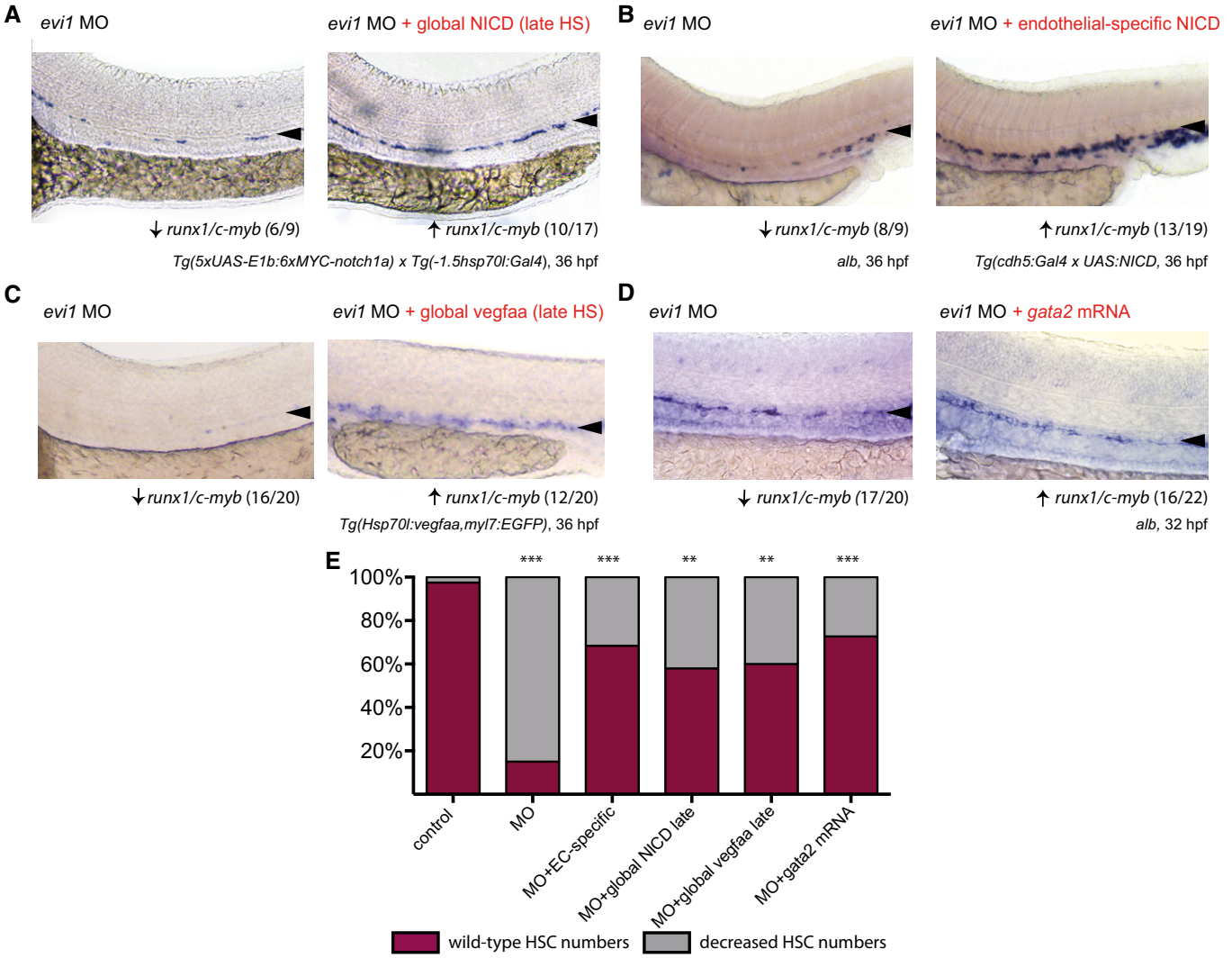

Figure 4. Global and tissue-specific activation of Notch or upstream Vegf signaling is sufficient to rescue HSPCs in *evi1* morphants.

A WISH for *runx1/c-myb* in 36 hpf *evi1* morphant (left) and *evi1* morphant transgenic *Tg(5xUAS-E1b:6xMYC-notch1a;-1.5hsp70l:Gal4)* embryos (right) with global heat-shock (HS) induction at 20 hpf.

B WISH for *runx1/c-myb* in 36 hpf *evi1* morphant (left) and *evi1* morphant transgenic *Tg(5xUAS-E1b:6xMYC-notch1a; cdh5:gal4ff)* embryos with endothelial-specific NICD induction (right).

C WISH for *runx1/c-myb* in 36 hpf *evi1* morphant (left) and *evi1* morphant transgenic *Tg(Hsp70l:vegfaa; myl7:eGFP)* embryos (right) with global heat-shock induction at 20 hpf.

D WISH for *runx1/c-myb* in 32 hpf *evi1* MO-injected embryos (left) and embryos injected with both *evi1* MO and capped *gata2* mRNA (right).

E Quantitation of all rescue experiments. Shown are the percentages of embryos displaying normal or changed *runx1/c-myb* expression. A Fisher's exact test was applied to calculate statistical significance. n.s., not significant; ***$P < 0.001$; **$P < 0.01$.

Data information: Data from three biological replicates are summarized for each experiment, with the exception of (D) where data from two experiments are shown. Lateral views are shown, anterior to the left, dorsal up. Numbers indicate the amount of embryos with the respective phenotype/total number of embryos analyzed in each experiment. Arrows indicate up- or downregulation of *runx1/c-myb* in each condition. Arrowheads denote the VDA region.

line (*Tg(cdh5^{BAC}:gal4ff)^{mu101}*) to induce NICD (*Tg(UAS:myc-Notch1a-intra)*). Indeed, forced NICD expression restricted to the endothelium was equally able to restore *runx1/c-myb* expression in the VDA of *evi1* morphants (Fig 4B and F). Moreover, the activation of Notch signaling (at both 14 or 20 hpf) via global induction of its upstream activator *vegfaa,* using a heat-shock inducible line (Carroll *et al*, 2014), also rescued HSPC development (Fig 4C and F, Appendix Figs S5B and C, and S6), while ectopic induction of the Notch target gene *gata2a,* via mRNA co-injection, provided a partial rescue (Fig 4D and F). Together, these data suggest that *evi1* induces EHT by regulating local Notch levels (see also Appendix Fig S7). To further explore this hypothesis, we performed live imaging analyses of *evi1* morphant fish with spatial-restricted endothelial expression of NICD (Fig 5A and B) by using an endothelial-specific Gal4 driver line (*Tg(fli.1:Gal4:RFP; c-myb:GFF)*) to induce NICD (*Tg(UAS:myc-Notch1a-intra)*). HSPCs directly emerging from *fli.1$^+$c-myb$^+$* cells in these fish were counted in $n = 5$ movies all from independent experiments taken over 8 h (Fig 5, Movies EV2 and EV3). Confirming our

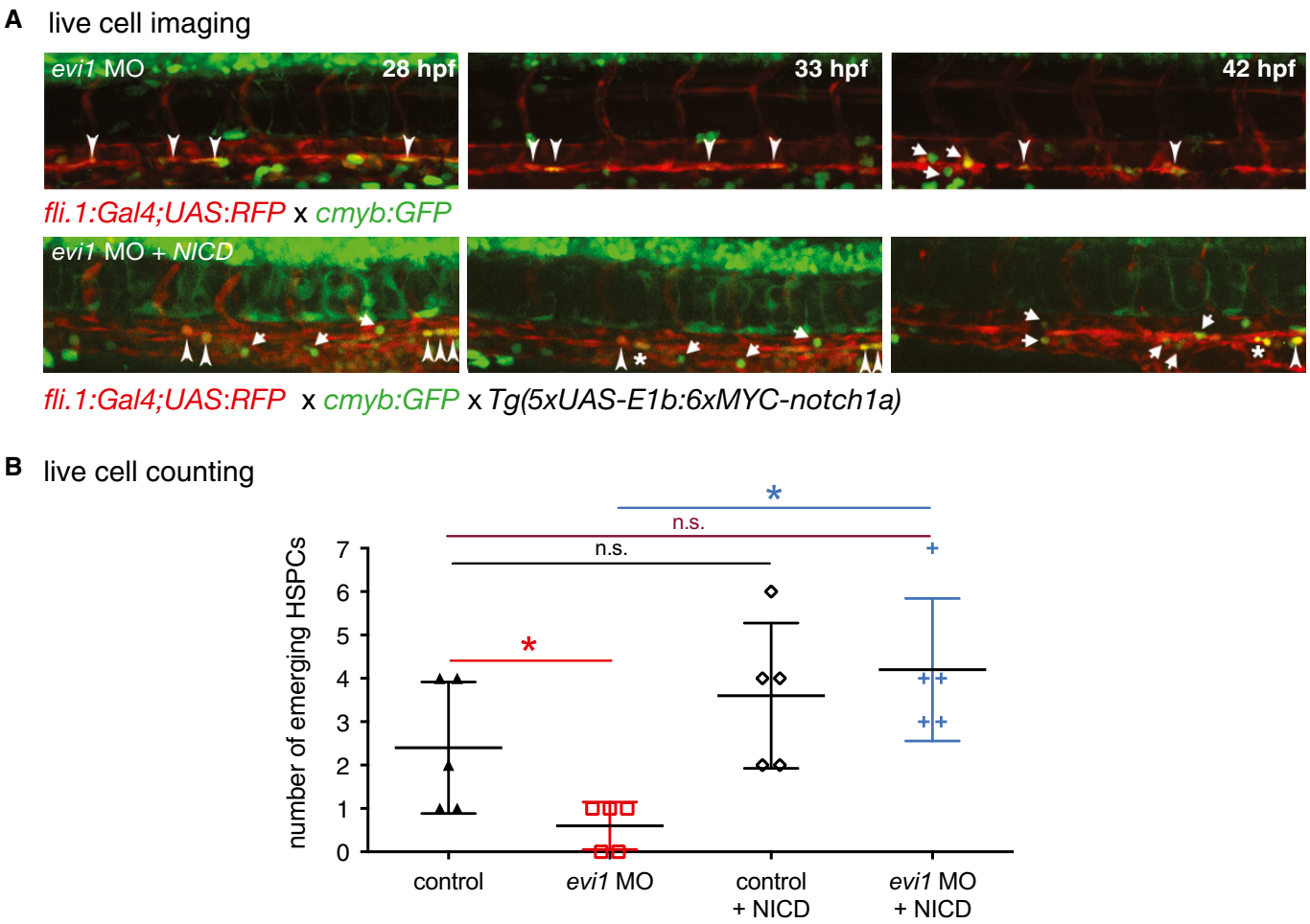

Figure 5. Endothelial NICD induction rescues HSC emergence from the VDA.

A Confocal time-lapse live imaging was performed in *Tg(c-myb:GFP; fli.1:UAS;Gal4:RFP) evi1* morphant embryos (top, Movie EV2) or in *Tg(c-myb:GFP; fli.1:UAS;Gal4:RFP)* crossed to *Tg(5xUAS-E1b:6xMYC-notch1a)* embryos prior to MO injection (bottom, Movie EV3) from 28 to 42 hpf. Shown are three representative time points, in which the transformation from hemogenic endothelial cells to the hematopoietic fate is visible. For each time point, merged images are shown. NICD induction controlled by endothelial *fli.1* (lower panel) can rescue the *evi1* morphant phenotype and increases the number of HSPCs cells emerging from the VDA (arrows). Arrowheads indicate double-positive cells. Dividing cells are marked by an asterisk.

B Cell counts of emerging HSPCs in control and *evi1* morphant fish with or without endothelial NICD induction. At least $n = 5$ movies from $n = 3$ biological replicates were analyzed. A nonparametric Mann–Whitney *U*-test was used to test for statistical significance, and error bars are shown as ± s.d. n.s., not significant, $*P < 0.05$.

previous results, *evi1* MO-injected embryos showed significantly lower numbers of HSPCs emerging from *fli.1*$^+$*c-myb*$^+$ cells of the endothelial niche, and enforced endothelial NICD expression could rescue these effects (Fig 5B, $P < 0.05$).

Since both ectopic NICD and its activator Vegf functionally rescued HSPC formation in *evi1* morphants, we next asked whether *evi1* controls Notch via Vegf. ISH for the Vegf receptor genes *flt1* and *flt4* as well as the known *vegf* upstream regulator *shh* showed unaltered expression upon *evi1* inhibition at 26 hpf (Fig EV3B and C). Moreover, whereas Vegf is critical for vasculature development (Liang *et al*, 2001), *evi1* morphants did not present overt vascular abnormalities, suggesting that *vegf* levels were not grossly influenced by *evi1* expression. Of note, overexpression of *vegfaa* not only restored the expression of *runx1/c-myb* (Fig 4C, Appendix Fig S5B and S6) but also of Notch pathway-associated molecules in the VDA of *evi1* morphants (*dll4*, *notch1b*, Fig 6A). In order to analyze whether *evi1* acts in parallel or downstream of Vegf, we next treated embryos with the Vegf receptor inhibitor SU5461 from 24 to 32 hpf. As expected, SU5461 treatment reduced *runx1/c-myb* and *notch1b* expression in the VDA in a dose-dependent manner (Fig 6B and C, middle and Appendix Fig S8). However, overexpression of *evi1* (achieved by co-injection of *UAS:mEvi1* in *Tg(fli.1:Gal4FF;UAS:RFP* embryos) was able to rescue *runx1*$^+$*/c-myb*$^+$ cells and *notch1b* expression in *evi1* MO-injected fish (Fig 6B and C, left). Together, these data indicate that *evi1* critically regulates EHT by activating Notch via a mechanism that is separate from and perhaps complementary to the classical *shh–vegf* axis.

evi1 activates endothelial Notch via pAKT

PI3K/AKT/mTOR signaling has been implicated in Notch regulation during development and is also known to be molecularly linked to

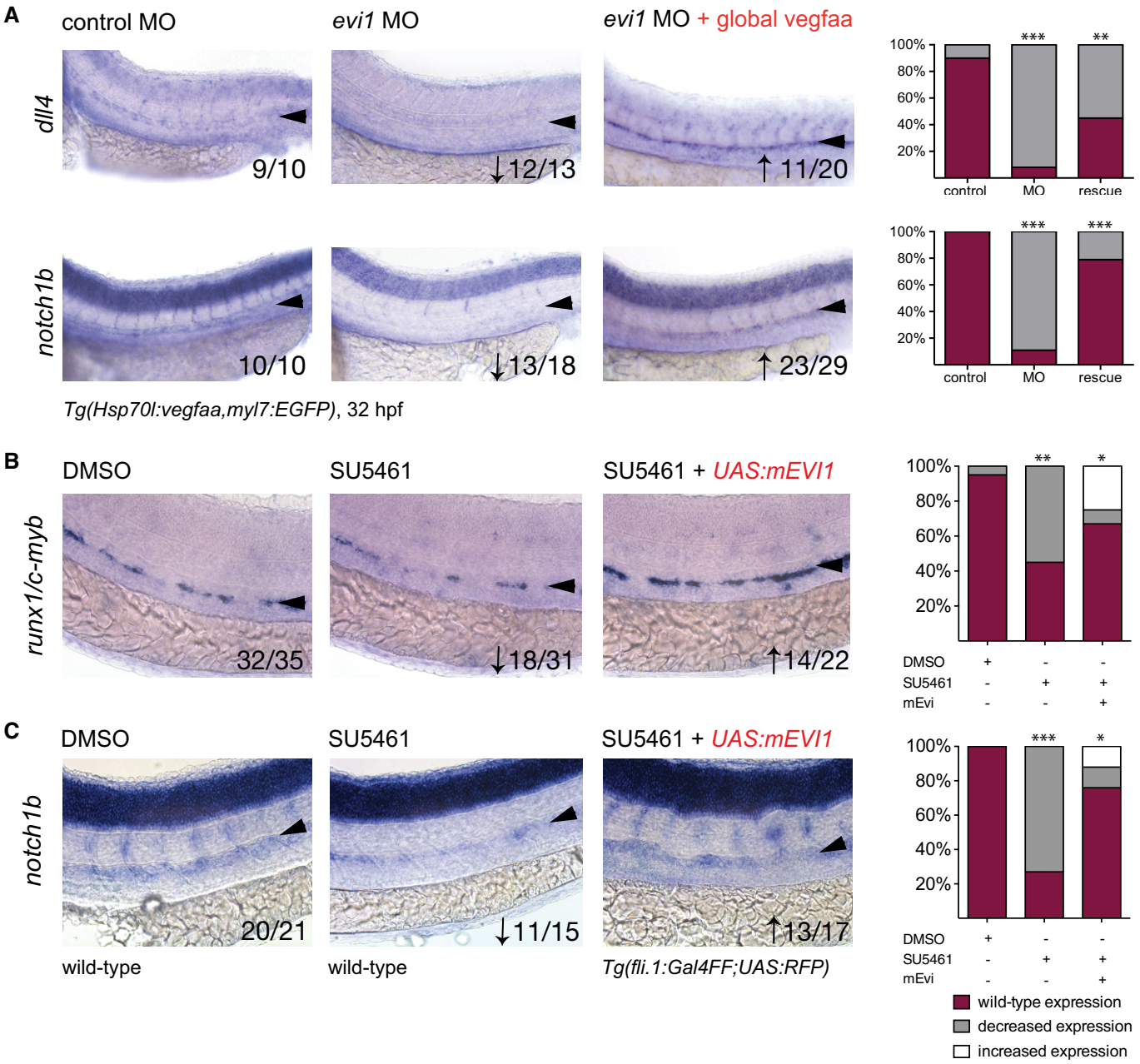

Figure 6. *evi1* regulates Notch independently of the Vegf pathway and can compensate for Vegf inhibition.

A WISH of *dll4* (upper) and *notch1b* (lower) in control-injected embryos (left), *evi1* morphants (middle), and *evi1* morphant transgenic *Tg(Hsp70l:vegfaa; myl7:eGFP)* embryos at 32 hpf after heat-shock induction at 20 hpf (right).

B, C WISH of *runx1/c-myb* (B) or *notch1b* (C) after treatment with DMSO (left), the VEGF receptor inhibitor SU5461 (middle), and, respectively, SU5461 after injection of *UAS:mEvi1* (inducing endothelial *evi1* expression) in *Tg(fli.1:Gal4FF;UAS:RFP)* embryos (right).

Data information: Two or more biological replicates are shown for each experiment. Lateral views are shown, anterior to the left, dorsal up. Numbers indicate the amount of embryos with the respective phenotype/total number of embryos analyzed in each experiment. Arrows indicate up- or downregulation of the respective gene in each condition. For each analyzed gene, quantitation of results is shown, displaying the percentages of embryos with normal vs. decreased gene expression for each condition. A Fisher's exact test was applied to calculate statistical significance (*$P < 0.05$, **$P < 0.01$, ***$P < 0.001$).

Evi1 in intestinal epithelial (Liu *et al*, 2006) and adult murine bone marrow cells (Yoshimi *et al*, 2011). Therefore, we sought to investigate the relationship between *evi1*, Notch, and AKT during HSC development. As shown in Fig 7A, embryos treated with the PI3Kγ inhibitor wortmannin (WM) from 14 to 36 hpf were analyzed for effects of pAKT suppression on *runx1/c-myb* expression in the VDA (Li *et al*, 2015). As observed in *evi1* morphants, vessel development remained intact, but expression of *runx1/c-myb* and *notch1b* was strongly suppressed in the VDA region upon treatment with WM (Fig 7A and B), reflective of efficiently suppressing pAKT

(Appendix Fig S9A). Importantly, enforced, heat-shock induced NICD expression was able to restore *runx1/c-myb* expression in WM-treated fish (Fig 7A, right), as previously documented in *evi1* MO-injected embryos (Fig 4A), suggesting these factors may work in conjunction to regulate Notch.

In adult hematopoietic cells, *Evi1* has been shown to positively regulate AKT phosphorylation via PTEN suppression (Yoshimi *et al*, 2011). Consistently, *evi1* morphants displayed suppressed pAKT but mainly unaltered AKT levels (Appendix Fig S9B, left and middle). However, no induction of PTEN protein levels were observed in *evi1* morphant vs. control-injected embryos (Appendix Fig S9B, right), suggesting that alternative regulatory mechanisms may be active. To further explore pAKT as a downstream target of *evi1* in VDA cells, rescue experiments were performed using a myristoylated AKT (myr-AKT) construct to induce pAKT in *evi1* morphants after heat-shock induction (Appendix Fig S9C and D). Indeed, mosaic expression of myr-AKT (Appendix Fig S9C and D) was sufficient to partially restore *runx1/c-myb* expression in the VDA of *evi1* MO-injected embryos (Fig 7C and D). Finally, forced endothelial pAKT expression, using a UAS:myr-AKT construct injected into *Tg(fli.1:Gal4FF^{ubs3}; UAS:RFP)^{rk}* embryos, rescued both *runx1/c-myb* and *notch1b* expressions (Fig 7C–E). In sum, these data indicate an endothelial *evi1*–pAKT molecular axis that acts in parallel to VEGF to control the precise induction of Notch expression levels required for HSPC emergence (Fig 7F).

Discussion

Evi1 has been primarily studied as an oncogene in myeloid and more recently lymphoid leukemia, as well as a marker of healthy and malignant hematopoietic stem cells (Suzukawa *et al*, 1994; Ogawa *et al*, 1996; Konantz *et al*, 2013; Sato *et al*, 2014; Saito & Morishita, 2015). *Evi1* and its target genes are preferentially expressed in long-term repopulating (LT)-HSCs, and *Evi1* has been functionally associated with stemness and self-renewal (Forsberg *et al*, 2010). Moreover, *Evi1* was shown to induce HSC proliferation via *Gata2* and apoptotic resistance as a target of *Survivin* (Yuasa *et al*, 2005; Goyama *et al*, 2008; Kataoka *et al*, 2011; Bard-Chapeau *et al*, 2014; Fukuda *et al*, 2015). This manuscript investigates the contribution of *evi1* to HSPC development during embryogenesis. *In vivo* loss-of-function studies were performed in zebrafish embryos, which, in contrast to mammalian embryos, develop *ex utero*, allowing direct visualization of HSC emergence. *evi1* suppression was achieved via the injection of inhibiting morpholino oligonucleotides. Notably, embryos injected with multiple gRNAs died, suggesting that introduction of mutations using the CRISPR-Cas9 system might be lethal even at mosaic levels. Consistent with murine *Evi1$^{-/-}$* AGM explant culture studies (Goyama *et al*, 2008) showing reduced HSC numbers, *evi1* zebrafish morphants displayed a profound suppression of VDA HSCs and consequently of definitive hematopoietic cells of all lineages *in vivo* (Fig 1). To explore the mechanistic role of *evi1* specifically on this cell population, we performed live imaging analysis on double-transgenic zebrafish embryos of the *Tg(kdrl:mKate-CAAX)* and *Tg(c-myb:eGFP)* lines, two marker previously used to visualize the generation of HSCs from the HE in the zebrafish VDA (Bertrand *et al*, 2010a; Kissa & Herbomel, 2010). Surprisingly, a yet unknown and very striking defect in HSPC specification from ECs was noted in detailed live imaging and molecular analyses of sorted cell populations, which all reinforced that indeed *evi1* promotes HSC development by controlling the completion of EHT and HSC emergence (Fig 3).

A major player required for HSPC formation is the *Notch* signaling pathway (Butko *et al*, 2016; Kanz *et al*, 2016), which is also important for the development of the VDA itself (Lawson *et al*, 2002; Quillien *et al*, 2014). As shown by multiple groups, Notch activity is mandatory to initiate specification of hematopoietic fate within the DA by controlling *runx1* expression (Kumano *et al*, 2003; Burns *et al*, 2005; Gering & Patient, 2005; Richard *et al*, 2013). *gata2b* expression within the hemogenic sub-compartment of the VDA is likewise *Notch*-dependent, and its deregulation reduces *runx1* (Butko *et al*, 2015). Upon *evi1* inhibition, downregulation of *notch1b* and *dll4* expressions was observed in VDA cells, although expression of the Notch target gene *efnb2a* was unchanged, indicating that cells have successfully undergone arterial specification (Figs 2A and EV4B). Moreover, production of EHT and HSPC was restored in *evi1* morphants by global or EC-specific induction of Notch, its upstream regulator Vegf, or its downstream target *gata2* (Fig 4). Together, these data indicate that *evi1* expression in EC is necessary for proper Notch signaling inducing EHT (Fig 5). In support of this hypothesis, the *Evi1* was recently found to be the second most upregulated transcription factor in murine AGM-derived HE as compared to EC cells (Solaimani Kartalaei *et al*, 2015). Furthermore, the Notch ligand *Dll4* has been lately demonstrated to mark human hemato-endothelial progenitor cells and regulate their hematopoietic fate (Ayllón *et al*, 2015; Gama-Norton *et al*, 2015). This signal is lacking

Figure 7. *evi1* regulates Notch signaling via pAKT.

A Expression of *runx1/c-myb* in the VDA after treatment with DMSO vehicle control (left), the PI3K/AKT inhibitor wortmannin (WM, middle), and after joined treatment with WM and enforced NICD expression via HS at 14 hpf in *Tg(5xUAS-E1b:6xMYC-notch1a;-1.5hsp70l:Gal4)* embryos (right). Graph displays quantitation of results. Shown are the percentages of embryos with normal or decreased *runx1/c-myb* expression for each condition.

B Expression of *notch1b* after treatment with DMSO vehicle control (left) or wortmannin (WM, middle). Graph displays quantitation of results. Shown are the percentages of embryos with normal or decreased *notch1b* expression for each condition.

C WISH for *runx1/c-myb* in control-injected embryos (upper left), *evi1* morphants (upper right), or, respectively, *evi1* MO with myr-AKT-injected embryos with HS at 14 hpf (lower right) and *evi1* MO with UAS:myr-AKT-injected transgenic *Tg(fli.1:Gal4FF^{ubs3}; UAS:RFP)^{rk}* embryos.

D Quantitation of results from (C). Shown are the percentages of embryos with normal or decreased *runx1/c-myb* expression for each condition.

E WISH for *notch1b* in *evi1* MO-injected (left) and *evi1* plus UAS:myr-AKT-injected transgenic *Tg(fli.1:Gal4FF^{ubs3}; UAS:RFP)^{rk}* embryos (right). Graph displays quantitation of results. Shown are the percentages of embryos with normal or decreased *notch1b* expression for each condition.

F Schematic illustration of the role of Evi1 during HSPC emergence and the dual regulation of Notch by the *shh–vegf* and the *evi1*–pAKT axes.

Data information: Two or more biological replicates are summarized for each experiment. Lateral views are shown, anterior to the left, dorsal up. Numbers indicate the amount of embryos with the respective phenotype/total number of embryos analyzed in each experiment. Arrows indicate up- or downregulation of each analyzed gene. A Fisher's exact test was applied to calculate statistical significance (n.s., not significant; *$P < 0.05$, **$P < 0.01$, ***$P < 0.001$).

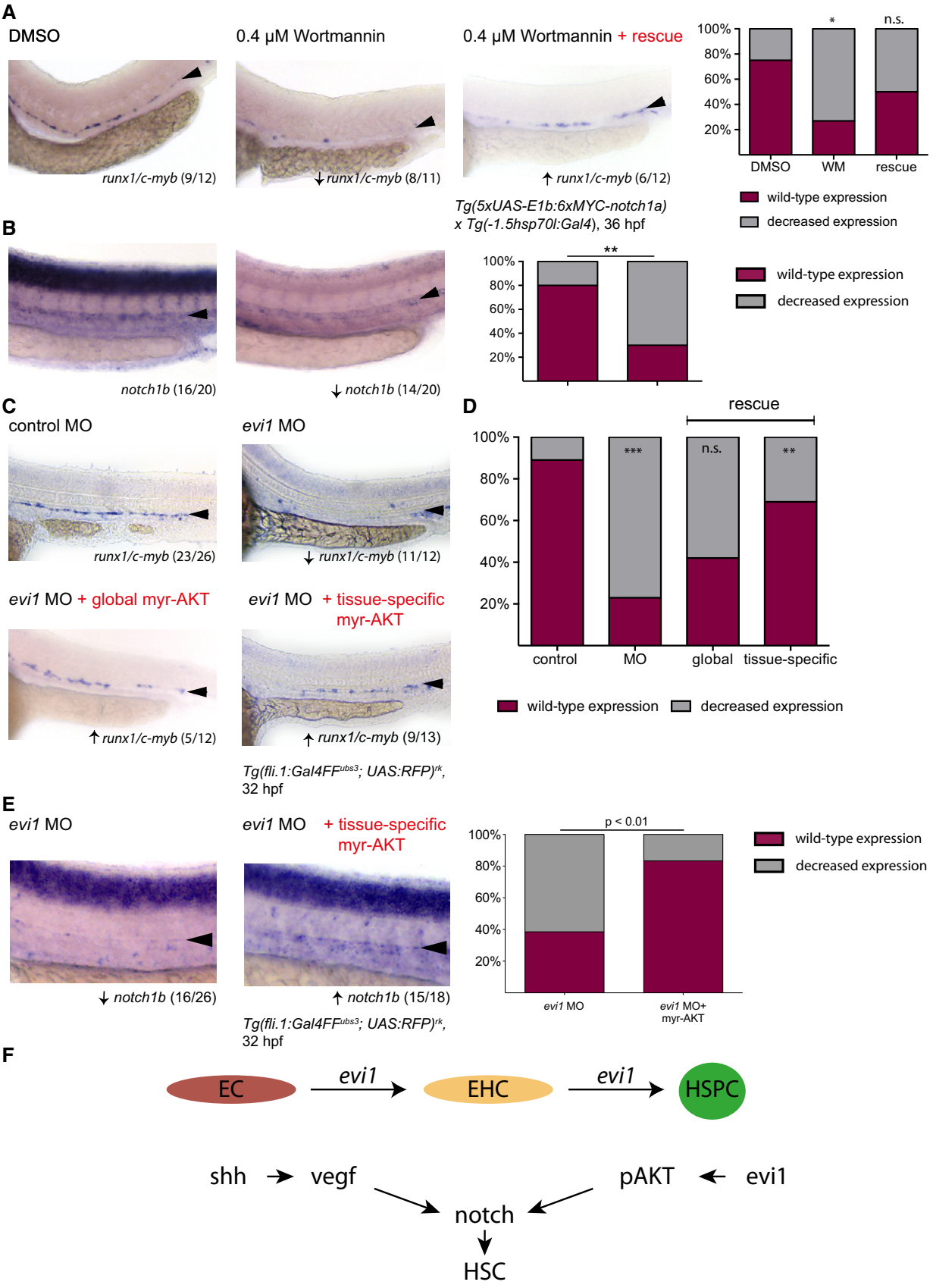
A
DMSO
0.4 μM Wortmannin
0.4 μM Wortmannin + rescue
runx1/c-myb (9/12)
↓runx1/c-myb (8/11)
↑runx1/c-myb (6/12)
100%
80%
60%
40%
20%
*
n.s.
DMSO
WM
rescue
wild-type expression
decreased expression
Tg(5xUAS-E1b:6xMYC-notch1a)
x Tg(-1.5hsp70l:Gal4), 36 hpf
B
notch1b (16/20)
↓notch1b (14/20)
**
C
control MO
evi1 MO
runx1/c-myb (23/26)
↓runx1/c-myb (11/12)
evi1 MO + global myr-AKT
evi1 MO + tissue-specific myr-AKT
↑runx1/c-myb (5/12)
↑runx1/c-myb (9/13)
Tg(fli.1:Gal4FFubs3; UAS:RFP)rk,
32 hpf
D
rescue
***
n.s.
**
control
MO
global
tissue-specific
E
evi1 MO
evi1 MO + tissue-specific myr-AKT
↓notch1b (16/26)
↑notch1b (15/18)
Tg(fli.1:Gal4FFubs3; UAS:RFP)rk,
32 hpf
p < 0.01
evi1 MO
evi1 MO+ myr-AKT
F
EC
evi1
EHC
evi1
HSPC
shh
vegf
pAKT
evi1
notch
HSC

Figure 7.

in *evi1* morphants, and therefore, we propose that EHT can initiate but then arrest in an intermediate state, with HE unable to generate emerging HSCs without Evi1 activity.

Recently, two separate waves of Notch signaling requirement have been identified for HSC development: an early somitic (~14 hpf), non-cell-autonomous and a late endothelial (~20 hpf), cell-autonomous wave (Clements *et al*, 2011; Kim *et al*, 2014). The fact that late induction of Notch (at 20 hpf) is sufficient to restore *runx1/c-myb* cell numbers and HSC emergence in our model strongly suggests that *evi1* regulates Notch levels required during this latter phase. Early induction of Notch at 14 hpf (via NICD or vegfaa) also provides a rescue (Appendix Fig S5), but in this experimental setting, induction is sustained throughout the second wave (20 hpf). In further support of the notion that *evi1* regulates the late Notch signaling requirement wave, *evi1* morphants showed unchanged expression of molecules shown to be involved during the first wave such as *wnt16*, downstream *dlc,* or of the sclerotome-specific markers *foxc1b* and *twist1b* (Fig EV4) (Clements *et al*, 2011; Kim *et al*, 2014). Finally, we show that *evi1* activates endothelial Notch independent of its well-known upstream regulator Vegf, since *evi1* expression restored Notch and HSPC numbers in embryos treated with the VEGF inhibitor SU5461. Consistently, Vegf-dependent endothelial development was unaffected in *evi1* morphants. We therefore propose that *evi1* induces activation of an alternative pathway that cooperates with Vegf to induce Notch levels permissive for EHT and HSC emergence.

A promising intermediate between Evi1 and Notch is the PI3K/AKT/mTOR signaling pathway. Mice with disrupted PI3K and Notch signaling show phenotypic similarities during blood development (Clayton *et al*, 2002), and co-culture with AKT-activated AGM-derived ECs was previously shown to stimulate the hematopoietic activity of E10-E11 P-Sp/AGM tissues (Hadland *et al*, 2015). Although more data exist on the role of Notch as an activator of the PI3K/AKT/mTOR pathway (Meurette *et al*, 2009; Cornejo *et al*, 2011), there is also evidence that, vice versa, PI3K/AKT can act upstream of *Notch*. For example, PI3K/AKT pathway activity has been shown to determine the cellular responsiveness to *Notch* signals in various cell types (McKenzie *et al*, 2006). Likewise, in T acute lymphoblastic leukemia (T-ALL) cells, AKT inhibitors could downregulate the expression of *Notch* pathway molecules (Calzavara *et al*, 2008). In our model, treatment with the PI3Kγ inhibitor wortmannin suppresses pAKT and strongly reduces both *notch1b* expression (Fig 7B) and *runx1/c-myb* expression in the VDA in a similar manner to that of *evi1* inhibition (Fig 7A, middle). Moreover, the *evi1* morphant/pAKT epistasis experiment confirmed that indeed *evi1* exerts its effects on Notch activity and subsequent EHT via modulation of endothelial pAKT (Fig 7C). In adult murine bone marrow, *Evi1* was shown to activate AKT/mTOR signaling by repressing PTEN either directly or via interaction with Polycomb group (PcG) proteins (Yoshimi *et al*, 2011). In spite showing reduction in pAKT, *evi1* morphants did not show convincing changes in PTEN levels, suggesting that *evi1* may modulate AKT phosphorylation by additional mechanisms (see Appendix Fig S9B). Finally, the G-coupled protein receptor 56 (Gpr56), a direct molecular target of *Evi1* in adult murine hematopoietic stem cells (Saito *et al*, 2013), has recently been identified by whole transcriptome analysis as a key factor in EHT in mice (Solaimani Kartalaei *et al*, 2015). In fish, HSCs were absent in *gpr56* morphants, and *gpr56* overexpression induced ectopic HSPC formation in the axial vein (Solaimani Kartalaei *et al*, 2015). How *gpr56* acts in the EHT and how it molecularly relates to the *evi1*–pAKT–*notch* molecular axis identified here is currently unknown and subject of ongoing studies. Recently, a related G protein-coupled receptor, *gpr183*, has also been found to regulate EHT in a Notch-dependent manner, indicating potential functional redundancies (Zhang *et al*, 2015).

Together, our study specifically addresses the function of Evi1 during HSC emergence from endothelial cells. Previous reports indicate that *Evi1* can regulate proliferation of fetal liver and bone marrow HSCs, thereby providing alternative mechanisms by which inhibition of this gene can impair stem cell numbers. Indeed, similar mechanisms of action during development as well as in the biology of preformed HSCs have been reported for *gata2*, a molecular downstream target of *evi1*. By taking advantage of the strengths of the zebrafish model for live imaging and genetic studies, we identify a novel Evi1–pAKT–Notch molecular axis that is essential for regulation of VDA EC, enabling EHT and subsequent HSC emergence during embryogenesis (Fig 7F).

Materials and Methods

Zebrafish husbandry and genetic strains

Zebrafish were bred and maintained as described in Nüsslein-Volhard & Dahm (2002) at 28°C. Staging was done by hours post-fertilization (hpf) as described by Warga and Kimmel (Warga & Kimmel, 1990) and according to FELASA and Swiss federal law guidelines. The following lines were used in this study: wild-type Tuebingen strains, *alb*, *Tg(globin: eGFP)*, *Tg(c-myb:GFP)* (both provided by L. I. Zon, Children's Hospital, Harvard Medical School, Boston, MA), *Tg(lyz:dsred)*, *Tg(cd41:eGFP)*, *Tg(UAS:myc-Notch1a-intra)^{kca3}*, *Tg(hsp70l:gal4)$^{1.5kca4}$*, *Tg(hsp:70l:vegfaa, myl7:eGFP)*, *Tg(cdh5^{BAC}:gal4ff)^{mu101}*, *Tg(BAC:kdrl:mKate2-CAAX)^{UBS16}*, and *Tg(fli.1:Gal4FF^{ubs3}; UAS:RFP)^{rk}* (Scheer & Campos-Ortega, 1999; Scheer *et al*, 2001; Lin *et al*, 2005; Hall *et al*, 2007; Parsons *et al*, 2009; Bussmann *et al*, 2011; Herwig *et al*, 2011; Wiley *et al*, 2011; Lenard *et al*, 2013).

Morpholino design and validation

Two *evi1* splice morpholino oligonucleotides (MO) and a standard control MO were synthesized by Gene Tools (Gene Tools LLC, OR, USA): (1: CCAAAATAGTGGTGTTCTCACCTCT, 2: TGAAGGGTCT GAGTGACTTACATAT), preventing either splicing of the first or the third exon–intron splice junction. Embryos were injected at the one-cell stage. About 0.05% of phenol red (Sigma-Aldrich, St. Louis, MI, USA) was added as an injection tracer. Embryos were raised to appropriate stages and fixed in 4% paraformaldehyde (PFA)/1× phosphate-buffered saline (PBS) for gene expression analysis. For validation, control-injected and MO-injected embryos were collected and mRNA was isolated using the RNeasy Mini Kit (Qiagen, Hilden, Germany). cDNA was synthesized using Transcriptor First Strand cDNA Synthesis Kit (Roche, Basel, Switzerland) according to the manufacturer's protocol. RT–PCR was performed using the following primers to verify splice modification on agarose gels: CAAGA

GAGATGGCCAAGGAG, GAGCAGGTCTTTCCTGATGC, ATAGTGCT TGCCGCTGTCAT, TATGAAGGGCTTGACGGAAG.

Generation of expression constructs

For rescue experiments, *evi1* and *gata2* were PCR-amplified using gene-specific primers (see Appendix Table S1), cloned into the pCR®2-TOPO® vector, and then subcloned into the pCS2+ expression vector. Capped RNA was synthesized using the mMessage mMachine SP6 Kit (Ambion Life Technologies, Carlsbad, CA, USA). About 25–45 picograms of RNA was injected into the yolk of one-cell stage embryos together with the *evi1* MO to rescue the MO phenotype. *UAS:mEvi1* was generated by cloning a codon-optimized version of the murine *Evi1* gene (Konantz *et al*, 2013) into pENTRY using the pENTRYD-TOPO cloning system (Invitrogen). pENTRY-mEvi1 and 4nrUAS (Akitake *et al*, 2011) were cloned into a Tol2 vector (pDestTol2CG2 (Kwan *et al*, 2007)). The final pUAS:mEvi1 plasmid was co-injected with tol2 mRNA into the *Tg(fli.1:Gal4F-F^{ubs3};UAS:RFP)^{rk}* and *Tg(-1.5hsp70l:Gal4)* embryos.

pBSFI-myr-akt1 was a gift from Peter Vogt (Addgene plasmid # 49186) (Aoki *et al*, 1998). To create the hsp70:myr-akt1 construct, gene-specific primers (see Appendix Table S1) with a 5′ BamHI and a 3′ BstBI restriction site were designed. Full-length myr-akt1 without the stop codon was PCR-amplified from the pBSFI-myr-akt1 plasmid as template and purified using the Wizard® SV Gel and PCR Clean-Up System (Promega, Fitchburg, WI, USA). After BamHI and BstBI digestion, the construct was subcloned in frame in a pMini Tol2 vector hsp70:cdc123 p2a Cherry (kindly provided by Judith Konantz, CRTD Dresden, Germany), substituting the cdc123 insert. Plasmid DNA containing the myr-Akt1 insert was injected into the zygote, and embryos were raised to the appropriate stage.

Whole-mount *in situ* hybridization (WISH) of zebrafish embryos

Riboprobes for WISH were generated using the following plasmid templates, restriction enzymes for DNA linearization, and RNA enzymes for further antisense probe production: *runx1*: HindIII, T7; *c-myb:* pBK-CMV, EcoRI, T7 (gift from Caroline E. Burns); *evi1*: pSPORT1, KpnI, SP6 (gift from Rebecca Wingert); *shh:* HindIII, T7 (gift from Judith Konantz); *rag1:* PCRII, HindIII, T7; *efnb2a*: pBS, HindII, T7; *foxn1:* XbaI, T7; *wnt16:* pCR2.1, NotI, SP6; *notch1b:* pCR-Script, BamHI, T3; *notch3:* pCR-Script, XhoI, T3; *dlc*: pBS(SK), XbaI, T7, *dll4:* PCRII, NotI, SP6; *twist1b:* pCRII, NotI, SP6, *foxc1b:* pCRII, BamHI, T7 (gifts from David Traver and Julien Bertrand); *flk1:* EcoRI, T7; *flt4:* EcoRI, T7 (gifts from Markus Affolter and Elin Ellertsdottir). RT/PCR-based approaches were used to generate riboprobes for *hbae3, mpo*, and *l-plastin* using gene-specific primers (Appendix Table S1). For the PCR, an antisense primer was designed, which has the T7-promoter sequence tagged onto its 5′-end. The resultant PCR product will then include the target sequence flanked by the T7-promoter sequence. Riboprobes were labeled with digoxigenin or fluorescein-labeled UTP as recommended by Roche, 100-fold diluted in Hyb solution, and stored at −20°C. WISH was performed according to standard procedures. Stained embryos were kept in 50% glycerol/PBS at 4°C until they were mounted in 89% glycerol and photographed using a digital AxioCam HRm camera attached on a Zeiss Axioplan 2 microscope or a digital MC170 HD camera attached to a Leica DM 2000 LED.

Flow cytometric analysis

Embryos were dissociated into single cells by using Accumax dissociation reagent (Millipore, Billerica, MA, USA) at room temperature. From time to time, embryos were disrupted using a 20-G needle. After dissociation was complete, cells were washed once in PBS and passed through a 35-μM filter. The number of fluorescent-labeled cells was them determined via flow cytometry on a FACSCanto II using FACSDiva™ software (BD Biosciences, Franklin Lakes, NJ, USA) and Sytox® blue for dead cell discrimination.

Isolation and time-lapse imaging of *kdrl$^+$c-myb$^+$* and, respectively, *fli.1$^+$c-myb$^+$* cells

Transgenic *Tg(c-myb:GFP)* were crossed to either *Tg(BAC:kdrl:mKate2-CAAX)^{UBS16} or Tg(fli1:Gal4FF; UAS:RFP)* fish. In order to isolate forming/emerging HSCs, embryos were screened for positive fluorescence, dissociated as described above, and sorted according to their fluorescence signal using a BD Influx™ Cell sorter. DAPI was used for live/dead cell discrimination. HSCs (*kdrl:mKate$^+$;c-myb:GFP$^+$*) were directly sorted into RNeasy lysis buffer (Qiagen), and RNA was isolated according to the manufacturer's protocol and amplified with QantiTect Whole Transcriptome Kit (Qiagen). Gene transcripts were detected by quantitative real-time reverse transcription PCR (qRT–PCR) using an Applied Biosystems® Real-Time PCR 7500 Fast System instrument and Fast Start Universal SYBR Green Master with Rox (Roche) and gene-specific primers (Appendix Table S1). A β-actin control for equal loading was used throughout the experiments to later normalize the real-time PCR data. Fold change values of gene expression between cells isolated from morphants vs. control embryos represented by averages from triplicate measurements were calculated using the $\Delta\Delta C_T$ method as described by Livak and Schmittgen (Livak & Schmittgen, 2001). For time-lapse imaging, fish were screened for fluorescence, anaesthetized in tricaine, and embedded in 0.8% low-melting agarose. Time-lapse imaging was performed using double-transgenic fish between 28 and 42 hpf on a Leica TCS SP5 confocal (*Tg(BAC:kdrl:mKate2-CAAX)^{UBS16} × Tg(c-myb:GFP)*) or a Visitron Systems CSU-W1 spinning disk microscope (*Tg(fli1:Gal4FF;UAS:RFP) × Tg(c-myb:GFP)*). Raw data were analyzed using Fiji software.

Rescue experiments

Tg(hsp70:gal4) were mated to *Tg(UAS:notch1a-intra)* and *Tg(hsp:70l:vegfaa,myl7:EGFP)* to wild-type Tuebingen stains, and (MO-injected) embryos were then raised in E3 until 14 hpf for heat-shock induction. Embryos were therefore collected in 5 ml of E3 and placed in a 38°C waterbath for 8 or 10 min, respectively. hsp70:myr-Akt p2a Cherry plasmid DNA-injected wild-type Tuebingen fish were heat-shocked in a 37°C water at the same age for 50 min. Subsequently, embryos were transferred to petri dishes and allowed to develop until the respective time points (26, 32, and 36 hpf) for further experiments. For tissue-specific rescue experiments *Tg(5xUAS-E1b:6xMYC-notch1a)*, fish were crossed to *Tg(cdh5^{BAC}:gal4ff)^{mu101}* animals prior to MO injection. For tissue-specific AKT rescue, UAS-AKT DNA (carrying *cmlc:GFP* as injection control; kind gift from M. Mione, Karlsruhe Institute

of Technology) was injected together with Tol2 RNA into *Tg(fli.1:Gal4FF^{ubs3}; UAS:RFP)^{rk}* embryos. For tissue-specific rescue *in vivo* live imaging experiments, *Tg(5xUAS-E1b:6xMYC-notch1a)* fish were crossed to *Tg(fliGal4:UAS:RFP;cmyb:GFP)* prior to MO injection. For rescue experiments with murine *Evi1*, the UAS-construct was injected with or without *evi1* MO in *Tg(fli.1:Gal4FF;UAS:RFP)* embryos.

Pharmacological inhibition of Notch, VEGF, and PI3K signaling

The γ-secretase inhibitor DAPT (Sigma-Aldrich) was dissolved in DMSO at 12.5 mM and applied at 100 μM as described before (Gering & Patient, 2005). The VEGF inhibitor SU5461 (Sigma-Aldrich) was applied between 24 and 32 hpf at different concentrations. To attenuate PI3K/AKT signaling, 0.4 μM wortmannin (Sigma) was added to 14 hpf embryos until the appropriate stage (Li *et al*, 2015). For each experiment, DMSO was used as a vehicle control.

Immunoblot analysis

Total protein lysates were prepared at the indicated times and after treatments by homogenizing between 10 and 50 embryos with an equal amount of lysis buffer. Lysates were denatured in Laemmli buffer and then electrophoresed on 12% polyacrylamide gels. After electrophoresis, proteins were transferred to PVDF membranes (Amersham, Amersham, UK) in a semi-dry blotting apparatus (Trans-Blot Turbo, Bio-Rad, Hercules, CA, USA) and then probed with the following antibodies: rabbit anti-human phospho-Akt (Ser473), anti-human pan Akt, anti-human PTEN, and anti β-actin from Cell Signaling Technology (Danvers, MA, USA) and detected via ECL.

o-Dianisidine staining

Whole embryo staining for heme expression was performed using o-dianisidine staining according to previously described methods (Detrich *et al*, 1995).

Expanded View for this article is available online.

Acknowledgements
We thank Loïc Sauteur, Judith Konantz, Christopher L. Antos, Caroline E. Burns, Leonard I. Zon, Julien Bertrand, David Traver, Rebecca Wingert, Marie Mayrhofer, Marina Mione, Markus Affolter, and Elin Ellertsdottir for critical reagents and Hui Wang, Tamara Pereboom, Sarah Hendel, the Imaging Core Facility of the Biozentrum Basel and the Department of Biomedicine (DBM), as well as the DBM Flow Cytometry Core Facility for technical support. This work was supported by grants from the Swiss National Science Foundation (SNF Project 149735), the Boehringer Ingelheim Fonds (Exploration Grant), and the Nora van Meeuwen Haefliger Stiftung to CL.

Author contributions
MK and CL wrote the paper. MK, EA, JM, and AL performed experiments and analyzed the data. MK, AL, EA, TEN, and CL analyzed and interpreted the data. VE, KJC, and LK provided critical reagents and/or technical/administrative support. All authors contributed to editing of the manuscript. CL conceived and supervised the study.

Conflict of interest
The authors declare that they have no conflict of interest.

References

Adamo L, Naveiras O, Wenzel PL, McKinney-Freeman S, Mack PJ, Gracia-Sancho J, Suchy-Dicey A, Yoshimoto M, Lensch MW, Yoder MC, García-Cardeña G, Daley GQ (2009) Biomechanical forces promote embryonic haematopoiesis. *Nature* 459: 1131 – 1135

Akitake CM, Macurak M, Halpern ME, Goll MG (2011) Transgenerational analysis of transcriptional silencing in zebrafish. *Dev Biol* 352: 191 – 201

Aoki M, Batista O, Bellacosa A, Tsichlis P, Vogt PK (1998) The akt kinase: molecular determinants of oncogenicity. *Proc Natl Acad Sci USA* 95: 14950 – 14955

Ayllón V, Bueno C, Ramos-Mejía V, Navarro-Montero O, Prieto C, Real PJ, Romero T, García-León MJ, Toribio ML, Bigas A, Menendez P (2015) The Notch ligand DLL4 specifically marks human hematoendothelial progenitors and regulates their hematopoietic fate. *Leukemia* 29: 1741 – 1753

Bard-Chapeau EA, Szumska D, Jacob B, Chua BQ, Chatterjee GC, Zhang Y, Ward JM, Urun F, Kinameri E, Vincent SD, Ahmed S, Bhattacharya S, Osato M, Perkins AS, Moore AW, Jenkins NA, Copeland NG (2014) Mice carrying a hypomorphic Evi1 allele are embryonic viable but exhibit severe congenital heart defects. *PLoS One* 9: e89397

Bertrand JY, Chi NC, Santoso B, Teng S, Stainier DY, Traver D (2010a) Haematopoietic stem cells derive directly from aortic endothelium during development. *Nature* 464: 108 – 111

Bertrand JY, Cisson JL, Stachura DL, Traver D (2010b) Notch signaling distinguishes 2 waves of definitive hematopoiesis in the zebrafish embryo. *Blood* 115: 2777 – 2783

Bertrand JY, Kim AD, Violette EP, Stachura DL, Cisson JL, Traver D (2007) Definitive hematopoiesis initiates through a committed erythromyeloid progenitor in the zebrafish embryo. *Development* 134: 4147 – 4156

Bertrand JY, Traver D (2009) Hematopoietic cell development in the zebrafish embryo. *Curr Opin Hematol* 16: 243 – 248

Boisset JC, van Cappellen W, Andrieu-Soler C, Galjart N, Dzierzak E, Robin C (2010) In vivo imaging of haematopoietic cells emerging from the mouse aortic endothelium. *Nature* 464: 116 – 120

de Bruijn MF, Speck NA, Peeters MC, Dzierzak E (2000) Definitive hematopoietic stem cells first develop within the major arterial regions of the mouse embryo. *EMBO J* 19: 2465 – 2474

Burns CE (2005) Hematopoietic stem cell fate is established by the Notch-Runx pathway. *Genes Dev* 19: 2331 – 2342

Burns CE, Galloway JL, Smith AC, Keefe MD, Cashman TJ, Paik EJ, Mayhall EA, Amsterdam AH, Zon LI (2009) A genetic screen in zebrafish defines a hierarchical network of pathways required for hematopoietic stem cell emergence. *Blood* 113: 5776 – 5782

Burns CE, Traver D, Mayhall E, Shepard JL, Zon LI (2005) Hematopoietic stem cell fate is established by the Notch-Runx pathway. *Genes Dev* 19: 2331 – 2342

Bussmann J, Wolfe SA, Siekmann AF (2011) Arterial-venous network formation during brain vascularization involves hemodynamic regulation of chemokine signaling. *Development* 138: 1717 – 1726

Butko E, Distel M, Pouget C, Weijts B, Kobayashi I, Ng K, Mosimann C, Poulain FE, McPherson A, Ni CW, Stachura DL, Del Cid N, Espín-Palazón R, Lawson ND, Dorsky R, Clements WK, Traver D (2015) Gata2b is a restricted

early regulator of hemogenic endothelium in the zebrafish embryo. *Development* 142: 1050 – 1061

Butko E, Pouget C, Traver D (2016) Complex regulation of HSC emergence by the Notch signaling pathway. *Dev Biol* 409: 129 – 138

Calzavara E, Chiaramonte R, Cesana D, Basile A, Sherbet GV, Comi P (2008) Reciprocal regulation of Notch and PI3K/Akt signalling in T-ALL cells in vitro. *J Cell Biochem* 103: 1405 – 1412

Carroll KJ, Esain V, Garnaas MK, Cortes M, Dovey MC, Nissim S, Frechette GM, Liu SY, Kwan W, Cutting CC, Harris JM, Gorelick DA, Halpern ME, Lawson ND, Goessling W, North TE (2014) Estrogen defines the dorsal-ventral limit of VEGF regulation to specify the location of the hemogenic endothelial niche. *Dev Cell* 29: 437 – 453

Chen AT, Zon LI (2009) Zebrafish blood stem cells. *J Cell Biochem* 108: 35 – 42

Chen MJ, Yokomizo T, Zeigler BM, Dzierzak E, Speck NA (2009) Runx1 is required for the endothelial to haematopoietic cell transition but not thereafter. *Nature* 457: 887 – 891

Clayton E, Bardi G, Bell SE, Chantry D, Downes CP, Gray A, Humphries LA, Rawlings D, Reynolds H, Vigorito E, Turner M (2002) A crucial role for the p110delta subunit of phosphatidylinositol 3-kinase in B cell development and activation. *J Exp Med* 196: 753 – 763

Clements WK, Kim AD, Ong KG, Moore JC, Lawson ND, Traver D (2011) A somitic Wnt16/Notch pathway specifies haematopoietic stem cells. *Nature* 474: 220 – 224

Cornejo MG, Mabialah V, Sykes SM, Khandan T, Lo Celso C, Lopez CK, Rivera-Muñoz P, Rameau P, Tothova Z, Aster JC, DePinho RA, Scadden DT, Gilliland DG, Mercher T (2011) Crosstalk between NOTCH and AKT signaling during murine megakaryocyte lineage specification. *Blood* 118: 1264 – 1273

Davidson AJ, Zon LI (2004) The 'definitive' (and 'primitive') guide to zebrafish hematopoiesis. *Oncogene* 23: 7233 – 7246

Delwel R, Funabiki T, Kreider BL, Morishita K, Ihle JN (1993) Four of the seven zinc fingers of the Evi-1 myeloid-transforming gene are required for sequence-specific binding to GA(C/T)AAGA(T/C)AAGATAA. *Mol Cell Biol* 13: 4291 – 4300

Detrich HW 3rd, Kieran MW, Chan FY, Barone LM, Yee K, Rundstadler JA, Pratt S, Ransom D, Zon LI (1995) Intraembryonic hematopoietic cell migration during vertebrate development. *Proc Natl Acad Sci USA* 92: 10713 – 10717

Forsberg EC, Passegue E, Prohaska SS, Wagers AJ, Koeva M, Stuart JM, Weissman IL (2010) Molecular signatures of quiescent, mobilized and leukemia-initiating hematopoietic stem cells. *PLoS One* 5: e8785

Fukuda S, Hoggatt J, Singh P, Abe M, Speth JM, Hu P, Conway EM, Nucifora G, Yamaguchi S, Pelus LM (2015) Survivin modulates genes with divergent molecular functions and regulates proliferation of hematopoietic stem cells through Evi-1. *Leukemia* 29: 433 – 440

Gama-Norton L, Ferrando E, Ruiz-Herguido C, Liu Z, Guiu J, Islam AB, Lee SU, Yan M, Guidos CJ, López-Bigas N, Maeda T, Espinosa L, Kopan R, Bigas A (2015) Notch signal strength controls cell fate in the haemogenic endothelium. *Nat Commun* 6: 8510

Gering M, Patient R (2005) Hedgehog signaling is required for adult blood stem cell formation in zebrafish embryos. *Dev Cell* 8: 389 – 400

Gori JL, Butler JM, Chan YY, Chandrasekaran D, Poulos MG, Ginsberg M, Nolan DJ, Elemento O, Wood BL, Adair JE, Rafii S, Kiem HP (2015) Vascular niche promotes hematopoietic multipotent progenitor formation from pluripotent stem cells. *J Clin Invest* 125: 1243 – 1254

Goyama S, Yamamoto G, Shimabe M, Sato T, Ichikawa M, Ogawa S, Chiba S, Kurokawa M (2008) Evi-1 is a critical regulator for hematopoietic stem cells and transformed leukemic cells. *Cell Stem Cell* 3: 207 – 220

Hadland BK, Varnum-Finney B, Poulos MG, Moon RT, Butler JM, Rafii S, Bernstein ID (2015) Endothelium and NOTCH specify and amplify aorta-gonad-mesonephros-derived hematopoietic stem cells. *J Clin Invest* 125: 2032 – 2045

Hall C, Flores MV, Storm T, Crosier K, Crosier P (2007) The zebrafish lysozyme C promoter drives myeloid-specific expression in transgenic fish. *BMC Dev Biol* 7: 42

Herwig L, Blum Y, Krudewig A, Ellertsdottir E, Lenard A, Belting HG, Affolter M (2011) Distinct cellular mechanisms of blood vessel fusion in the zebrafish embryo. *Curr Biol* 21: 1942 – 1948

Hirai H (1999) The transcription factor Evi-1. *Int J Biochem Cell Biol* 31: 1367 – 1371

Hoyt PR, Bartholomew C, Davis AJ, Yutzey K, Gamer LW, Potter SS, Ihle JN, Mucenski ML (1997) The Evi1 proto-oncogene is required at midgestation for neural, heart, and paraxial mesenchyme development. *Mech Dev* 65: 55 – 70

Jin H, Xu J, Wen Z (2007) Migratory path of definitive hematopoietic stem/progenitor cells during zebrafish development. *Blood* 109: 5208 – 5214

Kanz D, Konantz M, Alghisi E, North TE, Lengerke C (2016) Endothelial-to-hematopoietic transition: notch-ing vessels into blood. *Ann N Y Acad Sci* 1370: 97 – 108

Kataoka K, Sato T, Yoshimi A, Goyama S, Tsuruta T, Kobayashi H, Shimabe M, Arai S, Nakagawa M, Imai Y, Kumano K, Kumagai K, Kubota N, Kadowaki T, Kurokawa M (2011) Evi1 is essential for hematopoietic stem cell self-renewal, and its expression marks hematopoietic cells with long-term multilineage repopulating activity. *J Exp Med* 208: 2403 – 2416

Kim AD, Melick CH, Clements WK, Stachura DL, Distel M, Panáková D, MacRae C, Mork LA, Crump JG, Traver D (2014) Discrete Notch signaling requirements in the specification of hematopoietic stem cells. *EMBO J* 33: 2363 – 2373

Kissa K, Herbomel P (2010) Blood stem cells emerge from aortic endothelium by a novel type of cell transition. *Nature* 464: 112 – 115

Konantz M, Andre MC, Ebinger M, Grauer M, Wang H, Grzywna S, Rothfuss OC, Lehle S, Kustikova OS, Salih HR, Handgretinger R, Fend F, Baum C, Kanz L, Quintanilla-Martinez L, Schulze-Osthoff K, Essmann F, Lengerke C (2013) EVI-1 modulates leukemogenic potential and apoptosis sensitivity in human acute lymphoblastic leukemia. *Leukemia* 27: 56 – 65

Kumano K, Chiba S, Kunisato A, Sata M, Saito T, Nakagami-Yamaguchi E, Yamaguchi T, Masuda S, Shimizu K, Takahashi T, Ogawa S, Hamada Y, Hirai H (2003) Notch1 but not Notch2 is essential for generating hematopoietic stem cells from endothelial cells. *Immunity* 18: 699 – 711

Kwan KM, Fujimoto E, Grabher C, Mangum BD, Hardy ME, Campbell DS, Parant JM, Yost HJ, Kanki JP, Chien CB (2007) The Tol2kit: a multisite gateway-based construction kit for Tol2 transposon transgenesis constructs. *Dev Dyn* 236: 3088 – 3099

Lawson ND, Vogel AM, Weinstein BM (2002) Sonic hedgehog and vascular endothelial growth factor act upstream of the Notch pathway during arterial endothelial differentiation. *Dev Cell* 3: 127 – 136

Lenard A, Ellertsdottir E, Herwig L, Krudewig A, Sauteur L, Belting HG, Affolter M (2013) In vivo analysis reveals a highly stereotypic morphogenetic pathway of vascular anastomosis. *Dev Cell* 25: 492 – 506

Lengerke C, Daley GQ (2005) Patterning definitive hematopoietic stem cells from embryonic stem cells. *Exp Hematol* 33: 971 – 979

Lengerke C, Schmitt S, Bowman TV, Jang IH, Maouche-Chretien L, McKinney-Freeman S, Davidson AJ, Hammerschmidt M, Rentzsch F, Green JB, Zon LI,

Daley GQ (2008) BMP and Wnt specify hematopoietic fate by activation of the Cdx-Hox pathway. *Cell Stem Cell* 2: 72 – 82

Lengerke C, Daley GQ (2010) Autologous blood cell therapies from pluripotent stem cells. *Blood Rev* 24: 27 – 37

Li P, Lahvic JL, Binder V, Pugach EK, Riley EB, Tamplin OJ, Panigrahy D, Bowman TV, Barrett FG, Heffner GC, McKinney-Freeman S, Schlaeger TM, Daley GQ, Zeldin DC, Zon LI (2015) Epoxyeicosatrienoic acids enhance embryonic haematopoiesis and adult marrow engraftment. *Nature* 523: 468 – 471

Liang D, Chang JR, Chin AJ, Smith A, Kelly C, Weinberg ES, Ge R (2001) The role of vascular endothelial growth factor (VEGF) in vasculogenesis, angiogenesis, and hematopoiesis in zebrafish development. *Mech Dev* 108: 29 – 43

Lin HF, Traver D, Zhu H, Dooley K, Paw BH, Zon LI, Handin RI (2005) Analysis of thrombocyte development in CD41-GFP transgenic zebrafish. *Blood* 106: 3803 – 3810

Liu Y, Chen L, Ko TC, Fields AP, Thompson EA (2006) Evi1 is a survival factor which conveys resistance to both TGFbeta- and taxol-mediated cell death via PI3K/AKT. *Oncogene* 25: 3565 – 3575

Livak KJ, Schmittgen TD (2001) Analysis of relative gene expression data using real-time quantitative PCR and the 2(-Delta Delta C(T)) Method. *Methods* 25: 402 – 408

McKenzie G, Ward G, Stallwood Y, Briend E, Papadia S, Lennard A, Turner M, Champion B, Hardingham GE (2006) Cellular Notch responsiveness is defined by phosphoinositide 3-kinase-dependent signals. *BMC Cell Biol* 7: 10

Meurette O, Stylianou S, Rock R, Collu GM, Gilmore AP, Brennan K (2009) Notch activation induces Akt signaling via an autocrine loop to prevent apoptosis in breast epithelial cells. *Cancer Res* 69: 5015 – 5022

Mucenski ML, Taylor BA, Ihle JN, Hartley JW, Morse HC 3rd, Jenkins NA, Copeland NG (1988) Identification of a common ecotropic viral integration site, Evi-1, in the DNA of AKXD murine myeloid tumors. *Mol Cell Biol* 8: 301 – 308

Müller R, Lengerke C (2009) Patient-specific pluripotent stem cells: promises and challenges. *Nat Rev Endocrinol* 5: 195 – 203

North T, Gu TL, Stacy T, Wang Q, Howard L, Binder M, Marin-Padilla M, Speck NA (1999) Cbfa2 is required for the formation of intra-aortic hematopoietic clusters. *Development* 126: 2563 – 2575

North TE, Goessling W, Peeters M, Li P, Ceol C, Lord AM, Weber GJ, Harris J, Cutting CC, Huang P, Dzierzak E, Zon LI (2009) Hematopoietic stem cell development is dependent on blood flow. *Cell* 137: 736 – 748

Nüsslein-Volhard C, Dahm R (2002) *Zebrafish: a practical approach*. New York: Oxford University Press

Ogawa S, Kurokawa M, Tanaka T, Mitani K, Inazawa J, Hangaishi A, Tanaka K, Matsuo Y, Minowada J, Tsubota T, Yazaki Y, Hirai H (1996) Structurally altered Evi-1 protein generated in the 3q21q26 syndrome. *Oncogene* 13: 183 – 191

Palis J, Yoder MC (2001) Yolk-sac hematopoiesis: the first blood cells of mouse and man. *Exp Hematol* 29: 927 – 936

Parsons MJ, Pisharath H, Yusuff S, Moore JC, Siekmann AF, Lawson N, Leach SD (2009) Notch-responsive cells initiate the secondary transition in larval zebrafish pancreas. *Mech Dev* 126: 898 – 912

Perkins AS, Fishel R, Jenkins NA, Copeland NG (1991) Evi-1, a murine zinc finger proto-oncogene, encodes a sequence-specific DNA-binding protein. *Mol Cell Biol* 11: 2665 – 2674

Quillien A, Moore JC, Shin M, Siekmann AF, Smith T, Pan L, Moens CB, Parsons MJ, Lawson ND (2014) Distinct Notch signaling outputs pattern the developing arterial system. *Development* 141: 1544 – 1552

Richard C, Drevon C, Canto PY, Villain G, Bollérot K, Lempereur A, Teillet MA, Vincent C, Rosselló Castillo C, Torres M, Piwarzyk E, Speck NA, Souyri M, Jaffredo T (2013) Endothelio-mesenchymal interaction controls runx1 expression and modulates the notch pathway to initiate aortic hematopoiesis. *Dev Cell* 24: 600 – 611

Robert-Moreno A, Espinosa L, de la Pompa JL, Bigas A (2005) RBPjkappa-dependent Notch function regulates Gata2 and is essential for the formation of intra-embryonic hematopoietic cells. *Development* 132: 1117 – 1126

Robert-Moreno A, Guiu J, Ruiz-Herguido C, Lopez ME, Ingles-Esteve J, Riera L, Tipping A, Enver T, Dzierzak E, Gridley T, Espinosa L, Bigas A (2008) Impaired embryonic haematopoiesis yet normal arterial development in the absence of the Notch ligand Jagged1. *EMBO J* 27: 1886 – 1895

Saito Y, Kaneda K, Suekane A, Ichihara E, Nakahata S, Yamakawa N, Nagai K, Mizuno N, Kogawa K, Miura I, Itoh H, Morishita K (2013) Maintenance of the hematopoietic stem cell pool in bone marrow niches by EVI1-regulated GPR56. *Leukemia* 27: 1637 – 1649

Saito Y, Morishita K (2015) Maintenance of leukemic and normal hematopoietic stem cells in bone marrow niches by EVI1-regulated GPR56. *Rinsho Ketsueki* 56: 375 – 383

Sato T, Goyama S, Kataoka K, Nasu R, Tsuruta-Kishino T, Kagoya Y, Nukina A, Kumagai K, Kubota N, Nakagawa M, Arai S, Yoshimi A, Honda H, Kadowaki T, Kurokawa M (2014) Evi1 defines leukemia-initiating capacity and tyrosine kinase inhibitor resistance in chronic myeloid leukemia. *Oncogene* 33: 5028 – 5038

Scheer N, Campos-Ortega JA (1999) Use of the Gal4-UAS technique for targeted gene expression in the zebrafish. *Mech Dev* 80: 153 – 158

Scheer N, Groth A, Hans S, Campos-Ortega JA (2001) An instructive function for Notch in promoting gliogenesis in the zebrafish retina. *Development* 128: 1099 – 1107

Solaimani Kartalaei P, Yamada-Inagawa T, Vink CS, de Pater E, van der Linden R, Marks-Bluth J, van der Sloot A, van den Hout M, Yokomizo T, van Schaick-Solerno ML, Delwel R, Pimanda JE, van IJcken WFJ, Dzierzak E (2015) Whole-transcriptome analysis of endothelial to hematopoietic stem cell transition reveals a requirement for Gpr56 in HSC generation. *J Exp Med* 212: 93 – 106

Suzukawa K, Parganas E, Gajjar A, Abe T, Takahashi S, Tani K, Asano S, Asou H, Kamada N, Yokota J (1994) Identification of a breakpoint cluster region 3′ of the ribophorin I gene at 3q21 associated with the transcriptional activation of the EVI1 gene in acute myelogenous leukemias with inv(3)(q21q26). *Blood* 84: 2681 – 2688

Warga RM, Kimmel CB (1990) Cell movements during epiboly and gastrulation in zebrafish. *Development* 108: 569 – 580

Wieser R (2007) The oncogene and developmental regulator EVI1: expression, biochemical properties, and biological functions. *Gene* 396: 346 – 357

Wiley DM, Kim JD, Hao J, Hong CC, Bautch VL, Jin SW (2011) Distinct signalling pathways regulate sprouting angiogenesis from the dorsal aorta and the axial vein. *Nat Cell Biol* 13: 686 – 692

Yoshimi A, Goyama S, Watanabe-Okochi N, Yoshiki Y, Nannya Y, Nitta E, Arai S, Sato T, Shimabe M, Nakagawa M, Imai Y, Kitamura T, Kurokawa M (2011) Evi1 represses PTEN expression and activates PI3K/AKT/mTOR via interactions with polycomb proteins. *Blood* 117: 3617 – 3628

You LR, Lin FJ, Lee CT, DeMayo FJ, Tsai MJ, Tsai SY (2005) Suppression of Notch signalling by the COUP-TFII transcription factor regulates vein identity. *Nature* 435: 98 – 104

Yuasa H, Oike Y, Iwama A, Nishikata I, Sugiyama D, Perkins A, Mucenski ML, Suda T, Morishita K (2005) Oncogenic transcription factor Evi1 regulates hematopoietic stem cell proliferation through GATA-2 expression. *EMBO J* 24: 1976 – 1987

Zhang P, He Q, Chen D, Liu W, Wang L, Zhang C, Ma D, Li W, Liu B, Liu F (2015) G protein-coupled receptor 183 facilitates endothelial-to-hematopoietic transition via Notch1 inhibition. *Cell Res* 25: 1093 – 1107

Zhong TP, Childs S, Leu JP, Fishman MC (2001) Gridlock signalling pathway fashions the first embryonic artery. *Nature* 414: 216 – 220